

## Review article

Karim Achouri\* and Christophe Caloz\*

# Design, concepts, and applications of electromagnetic metasurfaces

<https://doi.org/10.1515/nanoph-2017-0119>

Received November 30, 2017; revised April 4, 2018; accepted April 6, 2018

**Abstract:** The paper overviews our recent work on the synthesis of metasurfaces and related concepts and applications. The synthesis is based on generalized sheet transition conditions (GSTCs) with a bianisotropic surface susceptibility tensor model of the metasurface structure. We first place metasurfaces in a proper historical context and describe the GSTC technique with some fundamental susceptibility tensor considerations. On this basis, we next provide an in-depth development of our susceptibility-GSTC synthesis technique. Finally, we present five recent metasurface concepts and applications, which cover the topics of birefringent transformations, bianisotropic refraction, light emission enhancement, remote spatial processing, and nonlinear second-harmonic generation.

**Keywords:** bianisotropy; electromagnetics; metasurfaces.

## 1 Introduction

Metamaterials reached a peak of interest in the first decade of the 21st century. Then, due to their fabrication complexity, bulkiness, and weight and their limitations in terms of losses, frequency range, and scalability, they became less attractive and were progressively superseded by their two-dimensional counterparts, the metasurfaces [1–5].

The idea of controlling electromagnetic waves with electromagnetically thin structures is clearly not a new concept. The first example is probably that of Lamb who studied the reflection and transmission from an array of metallic strips, already back in 1897 [6]. Later, in the

1910s, Marconi used arrays of straight wires to realize polarization reflectors [7]. These first two-dimensional electromagnetic structures were later followed by a great diversity of systems that emerged mainly with the developments of the radar technology during World War II. Many of these systems date back to the 1960s. The Fresnel zone plate reflectors, illustrated in Figure 1A, were based on the concept of the Fresnel lens demonstrated almost 150 years earlier and used in radio transmitters [8]. The frequency-selective surfaces (FSS), illustrated in Figure 1B, were developed as spatial filters [9, 10]. The reflectarray antennas [11] were developed as the flat counterparts of parabolic reflectors and were initially formed by short-ended waveguides [12]. They were later progressively improved and the short-ended waveguides were replaced with microstrip printable scattering elements in the late 1970s [13, 14], as shown in Figure 1C. The transmissive counterparts of the reflectarrays are the transmitarrays, which were used as array lens systems and date back to the 1960s [15–17]. They were first implemented in the form of two interconnected planar arrays of dipole antennas, one for receiving and one for transmitting, where each antenna on the receiver side was connected via a delay line to an antenna on the transmit side, as depicted in Figure 1D. Through the 1990s, the transmitarrays evolved from interconnected antenna arrays to layered metallic structures that were essentially the functional extensions of FSS [18–20] with efficiency limited by the difficulty to control the transmission phase over a  $2\pi$  range while maintaining a high enough amplitude. Finally, compact quasi-transparent transmitarrays or phase-shifting surfaces, able to cover a  $2\pi$ -phase range, were demonstrated in 2010 [21].

The aforementioned Fresnel lenses, FSS, reflectarrays, and transmitarrays are the precursors of today's "metasurfaces".<sup>1</sup>

\*Corresponding authors: Karim Achouri and Christophe Caloz, Department of Electrical Engineering, École Polytechnique de Montréal, Montréal, QC H3T 1J4, Canada, e-mail: karim.achouri@polymtl.ca (K. Achouri); christophe.caloz@polymtl.ca (C. Caloz). <http://orcid.org/0000-0002-6444-5215> (K. Achouri)

<sup>1</sup> Thus far, and throughout this paper, we essentially consider metasurfaces illuminated by waves incident on them under a nonzero angle with respect to their plane, i.e. space waves, which represent the metasurfaces leading to the main applications. However, metasurface may also be excited within their plane, i.e. by surface waves or leaky waves, as in Refs. [22–26].

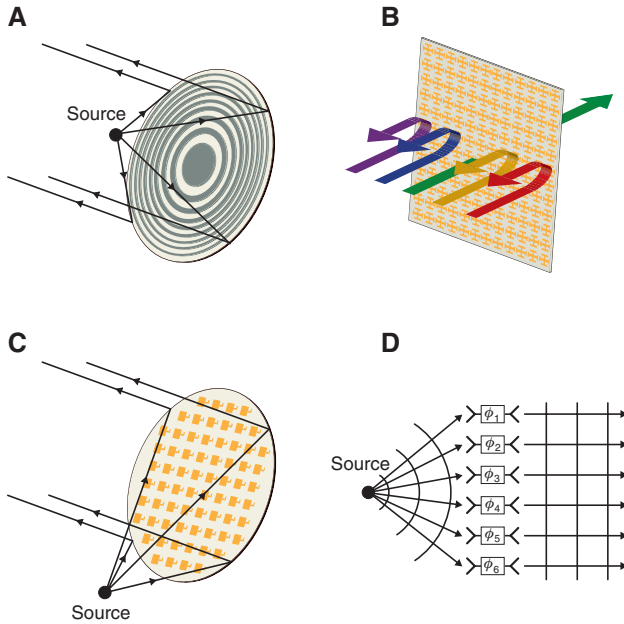


**Figure 1:** Examples of two-dimensional wave manipulating structures: (A) Fresnel zone plate reflector, (B) reflectarray, (C) interconnected array lens, and (D) FSS.

From a general perspective, metasurfaces can be used to manipulate the polarization, the phase, and the amplitude of electromagnetic fields. A rich diversity of metasurface applications has been reported in the literature to date and many more are expected to emerge. These applications are too numerous to be exhaustively cited. Some of the most significant ones are reported in Refs. [27–35] (polarization transformations), Refs. [36–42] (absorption), and Refs. [43–56] (wavefront manipulations). More sophisticated metasurfaces, transforming both phase and polarization, have been recently realized. This includes metasurfaces producing beams possessing angular orbital momentum [57] or vortex waves [58–63], holograms [64, 65], and stable beam traction [66]. Additionally, nonreciprocal transformations [67–71], nonlinear interactions [72–74], analog computing [75, 76], and spatial filtering [77–79] have also been reported.

To deploy their full potential, metasurfaces must be designed efficiently. This requires a solid “model” that both simplifies the actual problem and provides insight into its physics. Metasurfaces are best modeled, according to Huygens principle, as “surface polarization current sheets” via continuous (locally homogeneous) bianisotropic surface susceptibility tensorial functions. Inserting the corresponding surface polarization densities into Maxwell equations results in electromagnetic sheet transition conditions, which consist in the key equations to solve in the design of metasurfaces.

The objective of this paper is twofold. First, it will present a general framework for the synthesis of the aforementioned metasurface surface susceptibility functions for arbitrary (amplitude, phase, polarization, propagation direction, and waveform) specified fields. From this point, the physical structure (material and geometry of the scattering particles, substrate parameters, and layer configuration, thickness, and size) is tediously but straightforwardly determined, after the discretization of the susceptibility functions, using scattering parameter mapping. The synthesis of metasurfaces has been the objective of many researches in recent years [42, 80–90]. Second, the paper will show how this synthesis framework provides a general perspective of the electromagnetic transformations achievable by metasurfaces and then present subsequent concepts and applications.

## 2 Sheet transition conditions

The general synthesis problem of a metasurface is represented in Figure 2. As mentioned in Section 1, the metasurface is modeled as an electromagnetic sheet (zero-thickness film).<sup>2</sup> In the most general case, a metasurface is

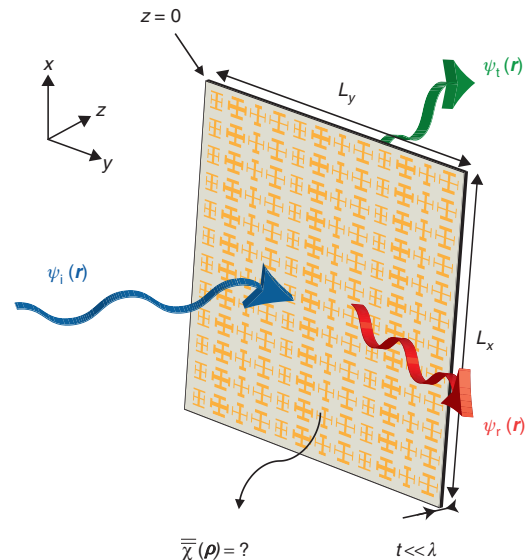


**Figure 2:** Metasurface synthesis problem.

The metasurface to be synthesized lies in the  $xy$ -plane at  $z=0$ . The synthesis procedure consists of finding the susceptibility tensors characterizing the metasurface,  $\bar{\chi}(\rho)$ , in terms of specified arbitrary incident  $[\psi_i(r)]$ , reflected  $[\psi_r(r)]$ , and transmitted  $[\psi_t(r)]$  waves.

<sup>2</sup> This approximation is justified by the fact that a physical metasurface is electromagnetically very thin, so that it cannot support significant phase shifts and related effects, such as Fabry-Perot resonances.

made of an array of polarizable scattering particles that induce both electric and magnetic field discontinuities. It is therefore necessary to express the discontinuities of these fields as functions of the electric and magnetic surface polarization densities ( $\mathbf{P}$  and  $\mathbf{M}$ ). The rigorous boundary conditions that apply to such an interface have been originally derived by Idemen [91].

For a metasurface lying in the  $xy$ -plane at  $z=0$ , these transition conditions follow from the idea that all the quantities in Maxwell equations can be expressed in the following form:

$$f(z) = \{f(z)\} + \sum_{k=0}^N f_k \delta^{(k)}(z), \quad (1)$$

where the function  $f(z)$  is discontinuous at  $z=0$ . The first term of the right-hand side of Eq. (1) is the “regular part” of  $f$ , which corresponds to the value of the function everywhere except at  $z=0$ , whereas the second term is the “singular part” of  $f$ , which is an expansion over the  $k$ th derivatives of the Dirac delta distribution (corresponding to the discontinuity of  $f$  and the  $k$ th derivatives of  $f$ ).

Most often, the series in Eq. (1) may be truncated at  $N=0$ , so that only the discontinuities of the fields are taken into account, whereas the discontinuities of the derivatives of the fields are neglected. With this truncation, the metasurface transition conditions, known as the generalized sheet transition conditions (GSTCs), are found as<sup>3</sup>

$$\hat{\mathbf{z}} \times \Delta \mathbf{H} = j\omega \mathbf{P}_{\parallel} - \hat{\mathbf{z}} \times \nabla_{\parallel} M_z, \quad (2)$$

$$\Delta \mathbf{E} \times \hat{\mathbf{z}} = j\omega \mu_0 \mathbf{M}_{\parallel} - \nabla_{\parallel} \left( \frac{P_z}{\epsilon_0} \right) \times \hat{\mathbf{z}}, \quad (3)$$

$$\hat{\mathbf{z}} \cdot \Delta \mathbf{D} = -\nabla \cdot \mathbf{P}_{\parallel}, \quad (4)$$

$$\hat{\mathbf{z}} \cdot \Delta \mathbf{B} = -\mu_0 \nabla \cdot \mathbf{M}_{\parallel}, \quad (5)$$

where the terms on the left-hand sides of the equations correspond to the differences of the fields on both sides of the metasurface, which may be expressed as

$$\Delta \Psi_u = \hat{\mathbf{u}} \cdot \Delta \Psi_{|z=0^+}^{0+} = \Psi_{u,t} - (\Psi_{u,i} + \Psi_{u,r}), \quad u = x, y, z, \quad (6)$$

where  $\Psi$  represents any of the fields  $\mathbf{E}$ ,  $\mathbf{H}$ ,  $\mathbf{D}$ , or  $\mathbf{B}$ , the subscripts  $i$ ,  $r$ , and  $t$  denote the incident, reflected, and

transmitted fields, and  $\mathbf{P}$  and  $\mathbf{M}$  are the electric and magnetic surface polarization densities, respectively.

In the general case of a linear bianisotropic metasurface, these polarization densities are related to the acting (or local) fields,  $\mathbf{E}_{\text{act}}$  and  $\mathbf{H}_{\text{act}}$ , by [93–95]:

$$\mathbf{P} = \epsilon_0 N \bar{\alpha}_{ee} \cdot \mathbf{E}_{\text{act}} + \frac{1}{c_0} N \bar{\alpha}_{em} \cdot \mathbf{H}_{\text{act}}, \quad (7)$$

$$\mathbf{M} = N \bar{\alpha}_{mm} \cdot \mathbf{H}_{\text{act}} + \frac{1}{\eta_0} N \bar{\alpha}_{me} \cdot \mathbf{E}_{\text{act}}, \quad (8)$$

where the  $\bar{\alpha}_{ab}$  tensors represent the polarizabilities of a given scatterer,  $N$  is the number of scatterers per unit area,  $c_0$  is the speed of light in vacuum, and  $\eta_0$  is the vacuum impedance.<sup>4</sup> This is a “microscopic” description of the metasurface response that requires an appropriate definition of the coupling between adjacent scattering particles. In this work, we use the concept of susceptibilities rather than the polarizabilities to provide a “macroscopic” description of the metasurface, which allows a direct connection with material parameters such as  $\bar{\epsilon}_r$  and  $\bar{\mu}_r$ . To bring about the susceptibilities, relations (7) and (8) can be transformed by noting that the acting fields, at the position of a scattering particle, can be defined as the average total fields minus the field scattered by the considered particle [97], i.e.  $\mathbf{E}_{\text{act}} = \mathbf{E}_{\text{av}} - \mathbf{E}_{\text{scat}}^{\text{part}}$ . The contributions of the particle may be expressed by considering the particle as a combination of electric and magnetic dipoles contained within a small disk, and the field scattered from this disk can be related to  $\mathbf{P}$  and  $\mathbf{M}$  by taking into account the coupling with adjacent scattering particles. Therefore, the acting fields are functions of the average fields and the polarization densities. Upon substitution of this definition of the acting fields in Eqs. (7) and (8), the expressions of the polarization densities become

$$\mathbf{P} = \epsilon_0 \bar{\chi}_{ee} \cdot \mathbf{E}_{\text{av}} + \frac{1}{c_0} \bar{\chi}_{em} \cdot \mathbf{H}_{\text{av}}, \quad (9)$$

$$\mathbf{M} = \bar{\chi}_{mm} \cdot \mathbf{H}_{\text{av}} + \frac{1}{\eta_0} \bar{\chi}_{me} \cdot \mathbf{E}_{\text{av}}, \quad (10)$$

where the average fields are defined as

$$\Psi_{u,\text{av}} = \hat{\mathbf{u}} \cdot \Psi_{\text{av}} = \frac{\Psi_{u,t} + (\Psi_{u,i} + \Psi_{u,r})}{2}, \quad u = x, y, z, \quad (11)$$

where  $\Psi$  corresponds to  $\mathbf{E}$  or  $\mathbf{H}$ .

<sup>4</sup> Despite being indeed quite general, these relations are still restricted to “linear” and “time-invariant” metasurfaces. The synthesis of nonlinear metasurfaces has been approached using extended GSTCs in Ref. [96].

<sup>3</sup> Note that these relations can also be obtained following the more traditional technique of box integration, as demonstrated in Ref. [92].

### 3 Susceptibility tensor considerations

Before delving into the metasurface synthesis, it is important to examine the susceptibility tensors in Eqs. (9) and (10) in the light of fundamental electromagnetic considerations pertaining to reciprocity, passivity, and loss.

The “reciprocity” conditions for a bianisotropic metasurface, resulting from the Lorentz theorem [93], read

$$\overline{\chi}_{ee}^T = \overline{\chi}_{ee}, \quad \overline{\chi}_{mm}^T = \overline{\chi}_{mm}, \quad \overline{\chi}_{me}^T = -\overline{\chi}_{em}, \quad (12)$$

where the superscript  $T$  denotes the matrix transpose operation.<sup>5</sup>

Adding the property of losslessness, resulting from the bianisotropic Poynting theorem [93], restricts Eq. (12) to

$$\overline{\chi}_{ee}^T = \overline{\chi}_{ee}^*, \quad \overline{\chi}_{mm}^T = \overline{\chi}_{mm}^*, \quad \overline{\chi}_{me}^T = \overline{\chi}_{em}^*, \quad (13)$$

which characterize a simultaneously passive, lossless, and reciprocal metasurface.

Conditions (12) and (13) establish relations between different susceptibility components of the constitutive tensors. Therefore, requiring the metasurface to be reciprocal or reciprocal and lossless/gainless, as often practically desirable, reduces the number of independent susceptibility components [80, 98, 99] and hence reduces the diversity of achievable field transformations, as will be shown next.

## 4 Metasurface synthesis

### 4.1 General concepts

We follow here the metasurface synthesis procedure<sup>6</sup> introduced in Ref. [80], which seems to be the most

general approach reported to date. This procedure consists of solving the GSTC equations (2)–(5) to determine the unknown susceptibilities in (9) and (10) required for the metasurface to perform the electromagnetic transformation specified in terms of the incident, reflected, and transmitted fields. Note that Eqs. (4) and (5) are redundant in system (2)–(5) due to the absence of impressed sources, so that Eqs. (2) and (3) are sufficient to fully describe the metasurface and synthesize it. Consequently, only the transverse (tangential to the metasurface) components of the specified fields, explicitly apparent in (6) and (11), are involved in the synthesis, although these fields may generally include longitudinal (normal to the metasurface) components as well. According to the uniqueness theorem, the longitudinal components of the fields are automatically determined from the transverse fields.

GSTC equations (2) and (3) form a set of (inhomogeneous) coupled partial differential equations due to the partial derivatives of the normal components of the polarization densities,  $P_z$  and  $M_z$ . The resolution of the corresponding inverse problem is nontrivial and requires involved numerical processing. In contrast, if  $P_z = M_z = 0$ , the differential system reduces to a simple algebraic system of equations, most conveniently admitting closed-form solutions for the synthesized susceptibilities. For this reason, we will focus on this case in this section, whereas a transformation example with nonzero normal susceptibilities will be discussed in Section 4.4.

Enforcing that  $P_z = M_z = 0$  may *a priori* seem to represent an important restriction, particularly, as we shall see, in the sense that it reduces the number of degrees of freedom of the metasurface. However, this is not a major restriction as a metasurface with normal polarization currents can generally be reduced to an equivalent metasurface with purely tangential polarization currents, according to Huygens theorem. This restriction mostly affects the realization of the scattering particles that are then forbidden to exhibit normal polarizations, which ultimately limits their practical implementation.<sup>7</sup>

<sup>5</sup> These conditions are identical to those for a bianisotropic medium [93, 94], except that the metasurfaces in Eq. (12) are surface instead of volume susceptibilities.

<sup>6</sup> The “synthesis” procedure consists of determining the physical metasurface structure for specified fields. The inverse procedure is the “analysis”, which consists of determining the fields scattered by a given physical metasurface structures for a given incident field and is generally coupled (typically iteratively) with the synthesis for the efficient design of a metasurface [100]. The overall design procedure thus consists of the combination of the synthesis and analysis operations. This paper focuses on the direct synthesis of the susceptibility functions, as this is the most important aspect for the understanding of the physical properties of metasurfaces, the elaboration of related concepts, and the development of resulting applications.

<sup>7</sup> Moreover, in the particular case where all the specified waves are normal to the metasurface, the excitation of normal polarization densities does not induce any discontinuity in the fields. This is because the corresponding fields, and hence the related susceptibilities, are not functions of the  $x$  and  $y$  coordinates, so that the spatial derivatives of  $P_z$  and  $M_z$  in Eqs. (2) and (3) are zero, i.e. do not induce any discontinuity in the fields across the metasurface. Thus, susceptibilities producing normal polarizations can be ignored, and only tangential susceptibility components must be considered, when the metasurface is synthesized for normal waves.

Substituting the constitutive relations (9) and (10) into the GSTCs (2) and (3) with  $M_z = P_z = 0$  leads to

$$\hat{\mathbf{z}} \times \Delta \mathbf{H} = j\omega\epsilon_0 \bar{\tilde{\chi}}_{ee} \cdot \mathbf{E}_{av} + jk_0 \bar{\tilde{\chi}}_{em} \cdot \mathbf{H}_{av}, \quad (14)$$

$$\Delta \mathbf{E} \times \hat{\mathbf{z}} = j\omega\mu_0 \bar{\tilde{\chi}}_{mm} \cdot \mathbf{H}_{av} + jk_0 \bar{\tilde{\chi}}_{me} \cdot \mathbf{E}_{av}, \quad (15)$$

where  $k_0 = \omega/c_0$  is the free-space wavenumber and where the susceptibility tensors only contain the tangential susceptibility components. This system can also be written in matrix form

$$\begin{pmatrix} \Delta H_y \\ \Delta H_x \\ \Delta E_y \\ \Delta E_x \end{pmatrix} = \begin{pmatrix} \tilde{\chi}_{ee}^{xx} & \tilde{\chi}_{ee}^{xy} & \tilde{\chi}_{em}^{xx} & \tilde{\chi}_{em}^{xy} \\ \tilde{\chi}_{ee}^{yx} & \tilde{\chi}_{ee}^{yy} & \tilde{\chi}_{em}^{yx} & \tilde{\chi}_{em}^{yy} \\ \tilde{\chi}_{me}^{xx} & \tilde{\chi}_{me}^{xy} & \tilde{\chi}_{mm}^{xx} & \tilde{\chi}_{mm}^{xy} \\ \tilde{\chi}_{me}^{yx} & \tilde{\chi}_{me}^{yy} & \tilde{\chi}_{mm}^{yx} & \tilde{\chi}_{mm}^{yy} \end{pmatrix} \cdot \begin{pmatrix} E_{x,av} \\ E_{y,av} \\ H_{x,av} \\ H_{y,av} \end{pmatrix}, \quad (16)$$

where the tilde symbol indicates normalized susceptibilities, related to the nonnormalized susceptibilities in (14) and (15) by

$$\begin{pmatrix} \chi_{ee}^{xx} & \chi_{ee}^{xy} & \chi_{em}^{xx} & \chi_{em}^{xy} \\ \chi_{ee}^{yx} & \chi_{ee}^{yy} & \chi_{em}^{yx} & \chi_{em}^{yy} \\ \chi_{me}^{xx} & \chi_{me}^{xy} & \chi_{mm}^{xx} & \chi_{mm}^{xy} \\ \chi_{me}^{yx} & \chi_{me}^{yy} & \chi_{mm}^{yx} & \chi_{mm}^{yy} \end{pmatrix} = \begin{pmatrix} \frac{j}{\omega\epsilon_0} \tilde{\chi}_{ee}^{xx} & \frac{j}{\omega\epsilon_0} \tilde{\chi}_{ee}^{xy} & \frac{j}{k_0} \tilde{\chi}_{em}^{xx} & \frac{j}{k_0} \tilde{\chi}_{em}^{xy} \\ -\frac{j}{\omega\epsilon_0} \tilde{\chi}_{ee}^{yx} & -\frac{j}{\omega\epsilon_0} \tilde{\chi}_{ee}^{yy} & -\frac{j}{k_0} \tilde{\chi}_{em}^{yx} & -\frac{j}{k_0} \tilde{\chi}_{em}^{yy} \\ -\frac{j}{k_0} \tilde{\chi}_{me}^{xx} & -\frac{j}{k_0} \tilde{\chi}_{me}^{xy} & -\frac{j}{\omega\mu_0} \tilde{\chi}_{mm}^{xx} & -\frac{j}{\omega\mu_0} \tilde{\chi}_{mm}^{xy} \\ \frac{j}{k_0} \tilde{\chi}_{me}^{yx} & \frac{j}{k_0} \tilde{\chi}_{me}^{yy} & \frac{j}{\omega\mu_0} \tilde{\chi}_{mm}^{yx} & \frac{j}{\omega\mu_0} \tilde{\chi}_{mm}^{yy} \end{pmatrix}. \quad (17)$$

System (16) contains four equations for 16 unknown susceptibilities. It is therefore heavily underdetermined and cannot be solved directly.<sup>8</sup> This leaves us with two distinct resolution possibilities.

The first possibility would be to reduce the number of susceptibilities from 16 to 4 to obtain a fully determined (full-rank) system. Because there exists many combinations of susceptibility quadruplets,<sup>9</sup> different sets can be

chosen, each of them naturally corresponding to different field transformations. This approach thus requires an educated selection of the susceptibility quadruplet that is the most likely to enable the specified operation, within existing constraints.<sup>10</sup>

These considerations immediately suggest that a second possibility would be to augment the number of field transformation specifications, i.e. allow the metasurface to perform more independent transformations, which may be of great practical interest in some applications. We would have thus ultimately three possibilities to resolve (16): (a) reducing the number of independent unknowns, (b) increasing the number of transformations, and (c) a combination of (a) and (b).

As we shall see in the forthcoming sections, the number  $\mathcal{N}$  of physically or practically achievable transformations for a metasurface with  $P$  susceptibility parameters,  $\mathcal{N}(P)$ , is not trivial; specifically,  $\mathcal{N}(P) = P/4$ , which may be expected from a purely mathematical viewpoint, is not always true.

## 4.2 Four-parameter transformation

We now provide an example for the approach where the number of susceptibility parameters has been reduced to 4, or  $P=4$ , so that system (16) is of full-rank nature. We thus have to select four susceptibility parameters and set all the others to zero in Eq. (17). We decide to consider the simplest case of a monoanisotropic (eight parameters  $\tilde{\chi}_{em,me}^{uv} = 0$ ,  $u, v = x, y$ ) axial (four parameters  $\tilde{\chi}_{ee,mm}^{uv} = 0$  for  $u \neq v$ ,  $u, v = x, y$ ) metasurface, which is thus characterized by the four parameters  $\tilde{\chi}_{ee}^{xx}$ ,  $\tilde{\chi}_{ee}^{yy}$ ,  $\tilde{\chi}_{mm}^{xx}$  and  $\tilde{\chi}_{mm}^{yy}$ , so that Eq. (16) reduces to the diagonal system:

$$\begin{pmatrix} \Delta H_y \\ \Delta H_x \\ \Delta E_y \\ \Delta E_x \end{pmatrix} = \begin{pmatrix} \tilde{\chi}_{ee}^{xx} & 0 & 0 & 0 \\ 0 & \tilde{\chi}_{ee}^{yy} & 0 & 0 \\ 0 & 0 & \tilde{\chi}_{mm}^{xx} & 0 \\ 0 & 0 & 0 & \tilde{\chi}_{mm}^{yy} \end{pmatrix} \cdot \begin{pmatrix} E_{x,av} \\ E_{y,av} \\ H_{x,av} \\ H_{y,av} \end{pmatrix}. \quad (18)$$

This metasurface is a “birefringent” structure [101], with decoupled  $x$ - and  $y$ -polarized susceptibility pairs

$$\chi_{ee}^{xx} = \frac{j\Delta H_y}{\omega\epsilon_0 E_{x,av}}, \quad \chi_{mm}^{yy} = \frac{j\Delta E_x}{\omega\mu_0 H_{y,av}} \quad (19)$$

and

<sup>10</sup> For instance, the specification of a reciprocal transformation, corresponding to the metasurface properties in Eq. (12), would automatically preclude the selection of off-diagonal pairs for  $\bar{\tilde{\chi}}_{ee,mm}$ .

<sup>8</sup> Even if it would be solved, this would probably result in an inefficient metasurface, as it would use more susceptibility terms than required to accomplish the specified task.

<sup>9</sup> Mathematically, the number of combinations would be  $16! / [(16-4)!4!] = 1820$ , but only a subset of these combinations represents physically meaningful combinations.

$$\chi_{ee}^{yy} = \frac{-j\Delta H_x}{\omega\epsilon_0 E_{y,av}}, \quad \chi_{mm}^{xx} = \frac{-j\Delta E_y}{\omega\mu_0 H_{x,av}}, \quad (20)$$

respectively.<sup>11</sup> In these relations, according to Eqs. (6) and (11),  $\Delta H_y = H_{y,t} - (H_{y,i} + H_{y,r})$ ,  $\Delta E_{x,av} = (E_{x,t} + E_{x,i} + E_{x,r})/2$ , and so on. By synthesis, the metasurface with the susceptibilities (19) and (20) will exactly transform the specified incident field into the specified reflected and transmitted fields, in an arbitrary fashion, except for the constraint of reciprocity as the susceptibility tensor in Eq. (18) inherently satisfies Eq. (12).

It should be noted that the example of Eq. (18), with four distinct susceptibility parameters, is a very particular case of a four-parameter transformation as the components in Eqs. (19) and (20) are decoupled from each other, which is the origin of birefringence. Now, birefringence may be considered as a “pair” of distinct and independent transformations (one for  $x$ -polarization and one for  $y$ -polarization), i.e.  $\mathcal{N}(4) = 2 > 4/4$ . Thus, the specification of four susceptibility parameters may lead to more than one transformation, which, by extension, already suggests that  $P$  susceptibilities may lead to more than  $P/4$  transformations, as announced in Section 4.1 and will be further discussed in Section 4.3.

Thus far, the fields have not been explicitly specified in the metasurface described by Eq. (18). Because the metasurface can perform arbitrary transformations under the reservation of reciprocity, it may for instance be used for polarization rotation, which will turn to be a most instructive example here. Consider the reflectionless metasurface, depicted in Figure 3, which transforms the polarization of a normally incident plane wave. The fields corresponding to this transformation are

$$\mathbf{E}_i(x, y) = \hat{\mathbf{x}} \cos(\pi/8) + \hat{\mathbf{y}} \sin(\pi/8), \quad (21)$$

$$\mathbf{H}_i(x, y) = \frac{1}{\eta_0} [-\hat{\mathbf{x}} \sin(\pi/8) + \hat{\mathbf{y}} \cos(\pi/8)], \quad (22)$$

$$\mathbf{E}_r(x, y) = 0, \quad (23)$$

$$\mathbf{H}_r(x, y) = 0, \quad (24)$$

and

<sup>11</sup> If the two electric and the two magnetic susceptibilities in (19) and (20) are equal to each other ( $\chi_{ee}^{xx} = \chi_{ee}^{yy}$  and  $\chi_{mm}^{xx} = \chi_{mm}^{yy}$ ), the monoanisotropic metasurface in Eq. (18) reduces to the simplest possible case of a monoanisotropic metasurface and hence performs the same operation for  $x$ - and  $y$ -polarized waves.

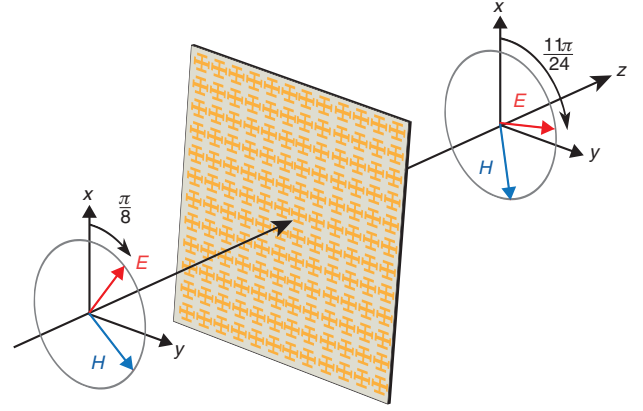


**Figure 3:** Polarization reflectionless rotating metasurface.

The metasurface rotates the polarization of a linearly polarized normally incident plane wave from the angle  $\pi/8$  to the angle  $11\pi/24$  with respect to the  $x$ -axis (rotation of  $\pi/3$ ). The metasurface is surrounded on both sides by vacuum, i.e.  $\eta_1 = \eta_2 = \eta_0$ .

$$\mathbf{E}_t(x, y) = \hat{\mathbf{x}} \cos(11\pi/24) + \hat{\mathbf{y}} \sin(11\pi/24), \quad (25)$$

$$\mathbf{H}_t(x, y) = \frac{1}{\eta_0} [-\hat{\mathbf{x}} \sin(11\pi/24) + \hat{\mathbf{y}} \cos(11\pi/24)]. \quad (26)$$

Inserting these fields into Eqs. (6) and (11) and substituting the result in (19) and (20) yields the susceptibilities

$$\chi_{ee}^{xx} = \chi_{mm}^{yy} = -\frac{1.5048}{k_0} j, \quad (27)$$

$$\chi_{ee}^{yy} = \chi_{mm}^{xx} = \frac{0.88063}{k_0} j. \quad (28)$$

Note that, in this example,<sup>12</sup> the aforementioned double transformation reduces to a single transformation,  $\mathcal{N}(4) = 1 = 4/4$ , because the specified fields possess both  $x$ - and  $y$ -polarizations. The susceptibilities do not depend on the position as the specified transformation, being purely normal, only rotates the polarization angle and does not affect the direction of wave propagation.

The negative and positive imaginary natures of  $\chi_{ee}^{xx} = \chi_{mm}^{yy}$  and  $\chi_{ee}^{yy} = \chi_{mm}^{xx}$  in (27) and (28) correspond to absorption and gain, respectively. These features may be understood by noting, with the help of Figure 3, that polarization rotation is accomplished here by attenuation

<sup>12</sup> Incidentally, the equality between the electric and magnetic susceptibilities results from the specification of zero reflection in addition to normal incidence. The reader may easily verify that, in the presence of reflection, the equalities do not hold.

and amplification of  $(E_{x,i}, H_{y,i})$  and  $(E_{y,i}, H_{x,i})$ , respectively. Moreover, this metasurface can rotate the polarization “only” by the angle  $\pi/3$  when the incident wave is polarized at a  $\pi/8$  angle.<sup>13</sup> This example certainly represents an awkward approach to rotate the field polarization.

A more reasonable approach is to consider a “gyrotropic” metasurface, where the only nonzero susceptibilities are  $\chi_{ee}^{xy}$ ,  $\chi_{ee}^{yx}$ ,  $\chi_{mm}^{xy}$  and  $\chi_{mm}^{yx}$ . This corresponds to a different quadruplet of tensor parameters than in Eq. (18), which illustrates the aforementioned multiplicity of possible parameter set selection. With these susceptibilities, system (16) yields the following relations:

$$\chi_{ee}^{xy} = \frac{j\Delta H_y}{\omega\epsilon_0 E_{y,av}}, \quad (29)$$

$$\chi_{ee}^{yx} = \frac{-j\Delta H_x}{\omega\epsilon_0 E_{x,av}}, \quad (30)$$

$$\chi_{mm}^{xy} = \frac{-j\Delta E_y}{\omega\mu_0 H_{y,av}}, \quad (31)$$

$$\chi_{mm}^{yx} = \frac{j\Delta E_x}{\omega\mu_0 H_{x,av}}, \quad (32)$$

which, upon substitution of the fields in (21) to (26), become

$$\chi_{ee}^{xy} = \chi_{mm}^{xy} = -\frac{1.1547}{k_0} j, \quad (33)$$

$$\chi_{ee}^{yx} = \chi_{mm}^{yx} = \frac{1.1547}{k_0} j. \quad (34)$$

Contrary to the susceptibilities in (27) and (28), those in (33) and (34) perform the specified  $\pi/3$  polarization rotation “irrespective” of the initial polarization of the incident wave due to the gyrotropic nature of the metasurface. It appears that these susceptibilities violate the reciprocity conditions in Eq. (12), and the metasurface is thus “nonreciprocal”, which is a necessary condition for polarization rotation with this choice of susceptibilities. Thus, the metasurface is a Faraday rotation surface,

whose direction of polarization rotation is independent of the direction of wave propagation [70, 102]. However, contrary to conventional Faraday rotators [93], this metasurface is also reflectionless due to the presence of both electric and magnetic gyrotropic susceptibility components (Huygens matching). The positive and negative imaginary susceptibilities indicate that the metasurface is simultaneously active and lossy, respectively. It is this combination of gain and loss that allows perfect rotation in this lossless design. This design is naturally appropriate if Faraday rotation is required. However, it is not optimal in applications not requiring nonreciprocity, i.e. reciprocal gyrotropy, where the required loss and gain would clearly represent a drawback.

Reciprocal gyrotropy may be achieved using bianisotropic chirality, i.e. which involves the parameter set  $\chi_{em}^{xx}$ ,  $\chi_{em}^{yy}$ ,  $\chi_{me}^{xx}$  and  $\chi_{me}^{yy}$ . Following the same synthesis procedure as before, we find

$$\chi_{em}^{xx} = \chi_{em}^{yy} = -\frac{2}{\sqrt{3}k_0} j, \quad (35)$$

$$\chi_{me}^{xx} = \chi_{me}^{yy} = \frac{2}{\sqrt{3}k_0} j. \quad (36)$$

The corresponding metasurface is readily verified to be reciprocal, passive, and lossless, as the susceptibility (35) and (36) satisfies condition (13). Therefore, if the purpose of the metasurface is to simply perform polarization rotation in a given direction, without specification for the opposite direction, this design is the most appropriate of the three discussed, as it is purely passive, lossless, and working for all incident polarizations.

Note that metasurfaces (33)–(36) correspond to  $\mathcal{N}(4) = 1 = 4/4$ .

### 4.3 More-than-four-parameter transformation

In the previous section, we have seen how system (16) can be solved by reducing the number of susceptibilities to  $P=4$  parameters to match the number of GSTCs equations and we have also seen some of the resulting single-transformation ( $\mathcal{N}=1$ , e.g. monoisotropic structure) or double-transformation ( $\mathcal{N}=2$ , e.g. birefringence) metasurface possibilities.

However, as mentioned in Section 4.1, the general system of equation (16), given its 16 degrees of freedom (16 susceptibility components), corresponds to a

<sup>13</sup> If, for instance, the incident was polarized along  $x$  only, then only the susceptibilities in Eq. (27) would be excited and the resulting transmitted field would still be polarized along  $x$ , just with a reduced amplitude with respect to that of the incident wave due to the loss induced by these susceptibilities.

metasurface with the potential capability to perform “more transformations” than a metasurface with 4 parameters, or generally less than 16 parameters,  $\mathcal{N}(16) > \mathcal{N}(P < 16)$ . In what follows, we will see how system (16) can be solved for several “independent” transformations, which includes the possibility of differently processing waves incident from either sides. To accommodate for the additional degrees of freedom, a total of four wave transformations are considered instead of only one as done in Section 4.2, so that (16) becomes a full-rank system. The corresponding equations related to system (16) may then be written in the compact form:

$$\begin{pmatrix} \Delta H_{y1} & \Delta H_{y2} & \Delta H_{y3} & \Delta H_{y4} \\ \Delta H_{x1} & \Delta H_{x2} & \Delta H_{x3} & \Delta H_{x4} \\ \Delta E_{y1} & \Delta E_{y2} & \Delta E_{y3} & \Delta E_{y4} \\ \Delta E_{x1} & \Delta E_{x2} & \Delta E_{x3} & \Delta E_{x4} \end{pmatrix} = \begin{pmatrix} \tilde{\chi}_{ee}^{xx} & \tilde{\chi}_{ee}^{xy} & \tilde{\chi}_{em}^{xx} & \tilde{\chi}_{em}^{xy} \\ \tilde{\chi}_{ee}^{yx} & \tilde{\chi}_{ee}^{yy} & \tilde{\chi}_{em}^{yx} & \tilde{\chi}_{em}^{yy} \\ \tilde{\chi}_{me}^{xx} & \tilde{\chi}_{me}^{xy} & \tilde{\chi}_{mm}^{xx} & \tilde{\chi}_{mm}^{xy} \\ \tilde{\chi}_{me}^{yx} & \tilde{\chi}_{me}^{yy} & \tilde{\chi}_{mm}^{yx} & \tilde{\chi}_{mm}^{yy} \end{pmatrix} \begin{pmatrix} E_{x1,av} & E_{x2,av} & E_{x3,av} & E_{x4,av} \\ E_{y1,av} & E_{y2,av} & E_{y3,av} & E_{y4,av} \\ H_{x1,av} & H_{x2,av} & H_{x3,av} & H_{x4,av} \\ H_{y1,av} & H_{y2,av} & H_{y3,av} & H_{y4,av} \end{pmatrix}, \quad (37)$$

where subscripts 1–4 indicate the electromagnetic fields corresponding to four distinct and “independent” sets of waves.<sup>14</sup> The susceptibilities can be obtained by matrix inversion conjointly with the normalization (17). The resulting susceptibilities will, in general, be all different from each other. This means that the corresponding metasurface is both active/lossy and nonreciprocal.

Consider, for example, a metasurface with  $P=8$  parameters. In such a case, system (16) is underdetermined as it features four equations in eight unknowns. This suggests the possibility to specify more than one transformation,  $\mathcal{N} > 1$ . Let us thus consider, for instance, a monoanisotropic (eight-parameter) metasurface and see whether such a metasurface can indeed perform

<sup>14</sup> It is also possible to solve a system of equations that contains less than these 16 susceptibility components. In that case, less than four wave transformations should be specified so that the system remains fully determined. For instance, two independent wave transformations (possessing both  $x$ - and  $y$ -polarizations) could be solved with eight susceptibilities. Similarly, three wave transformations could be solved with 12 susceptibilities.

two transformations. The corresponding system for two transformation reads

$$\begin{pmatrix} \Delta H_{y1} & \Delta H_{y2} \\ \Delta H_{x1} & \Delta H_{x2} \\ \Delta E_{y1} & \Delta E_{y2} \\ \Delta E_{x1} & \Delta E_{x2} \end{pmatrix} = \begin{pmatrix} \tilde{\chi}_{ee}^{xx} & \tilde{\chi}_{ee}^{xy} & 0 & 0 \\ \tilde{\chi}_{ee}^{yx} & \tilde{\chi}_{ee}^{yy} & 0 & 0 \\ 0 & 0 & \tilde{\chi}_{mm}^{xx} & \tilde{\chi}_{mm}^{xy} \\ 0 & 0 & \tilde{\chi}_{mm}^{yx} & \tilde{\chi}_{mm}^{yy} \end{pmatrix} \begin{pmatrix} E_{x1,av} & E_{x2,av} \\ E_{y1,av} & E_{y2,av} \\ H_{x1,av} & H_{x2,av} \\ H_{y1,av} & H_{y2,av} \end{pmatrix}. \quad (38)$$

This system (38), being full-rank, automatically admits a solution for the eight susceptibilities, i.e.  $\mathcal{N}=2$ . The only question is whether this solution complies with practical design constraints. For instance, the electric and magnetic susceptibility submatrices are nondiagonal and may therefore violate the reciprocity condition (12). If nonreciprocity is undesirable or unrealizable in a practical situation, then one would have to try another set of eight parameters.

If this eight-parameter metasurface performs only two transformations, then one may wonder what is the difference with the four-parameter birefringent metasurface in Eq. (18), which can also provide two transformations with just four parameters. The difference is that the two-transformation property of the metasurface in Eq. (18) is restricted to the case where the fields of the two transformations are orthogonally polarized,<sup>15</sup> whereas the two-transformation property of the metasurface in Eq. (38) is completely general.

As an illustration of the latter metasurface, consider the two transformations depicted in Figure 4. The first transformation, shown in Figure 4A, consists of reflecting at  $45^\circ$  a normally incident plane wave. The second transformation, shown in Figure 4B, consists of fully absorbing an incident wave impinging on the metasurface under  $45^\circ$ . In both cases, the transmitted field is specified to be zero for the first and second transformations. The transverse components of the electric fields for the two transformations are, at  $z=0$ , given by

$$\mathbf{E}_{i,1} = \frac{\sqrt{2}}{2}(\hat{\mathbf{x}} + \hat{\mathbf{y}}), \quad \mathbf{E}_{i,2} = \frac{\sqrt{2}}{2}(-\cos\theta_r \hat{\mathbf{x}} + \hat{\mathbf{y}})e^{-jk_r x}, \quad (39)$$

<sup>15</sup> For instance, if the fields of the first transformation are only  $x$ -polarized, the fields of the second transformation are only  $y$ -polarized.

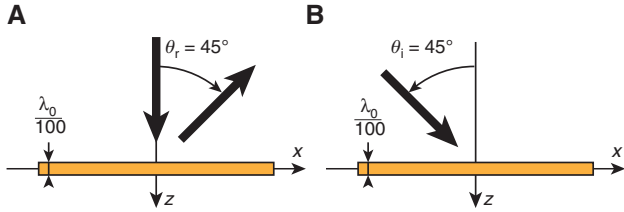


**Figure 4:** Example of double-transformation metasurface: (A) first transformation [corresponding to subscript 1 in Eq. (38)]: the normally incident plane wave is fully reflected at a  $45^\circ$  angle and (B) second transformation [corresponding to subscript 2 in Eq. (38)]: the obliquely incident plane wave is fully absorbed.

$$\mathbf{E}_{i,2} = \frac{\sqrt{2}}{2}(\cos\theta_i \hat{\mathbf{x}} + \hat{\mathbf{y}})e^{-jk_x x}, \quad (40)$$

respectively.

The synthesis is then performed by inserting the electric field (39) and (40), and the corresponding magnetic fields, into Eq. (38). The susceptibilities are then straightforwardly obtained by matrix inversion in Eq. (38). For the sake of conciseness, we do not give them here, but we point out that they include nonreciprocity, loss and gain, and complex spatial variations.

This double-transformation response is verified by full-wave simulation and the resulting simulations are plotted in Figure 5. The two simulations in this figure have been realized in the commercial FEM software

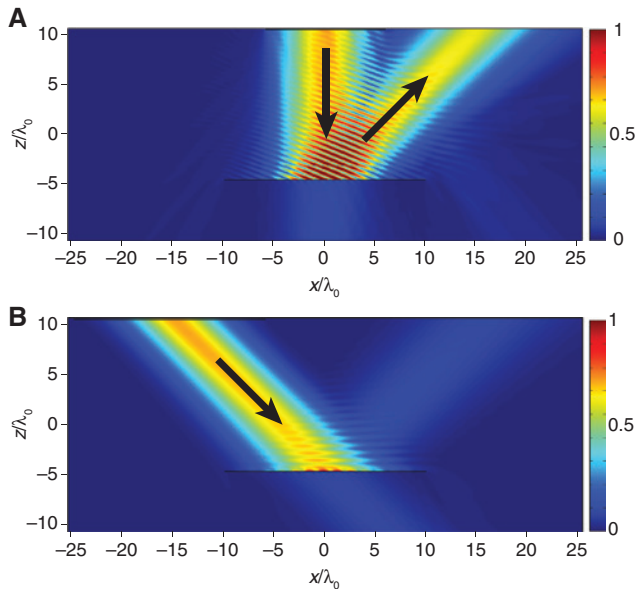


**Figure 5:** Eight-parameter metasurface simulations: COMSOL simulated normalized absolute value of the total electric field corresponding to (A) the transformation in Figure 4A and (B) the transformation in Figure 4B.

COMSOL, where the metasurface is implemented as a thin material slab of thickness  $d = \lambda_0/100$ .<sup>16</sup> The simulation corresponding to the transformation of Figure 4A is shown in Figure 5A, whereas the simulation corresponding to the transformation of Figure 4B is shown in Figure 5B. The simulated results are in agreement with the specification [Eqs. (39) and (40)], except for some scattering due to the nonzero thickness of the full-wave slab approximation.

The example just presented, where both transformations 1 and 2 include all the components of the fields, corresponds to  $\mathcal{N}(8) = 2 = 8/4$ , i.e.  $\mathcal{N}(P) = P/4$ . However, in the same manner as the birefringent metasurface of (19) and (20), featuring  $\mathcal{N}(4) = 2 > 4/4$ , i.e. specifically  $\mathcal{N}(P) = P/2$ , the metasurface in Eq. (38) may lead to  $\mathcal{N}(P) > P/4$ . This depends essentially on whether the specified transformations are composed of fields that are either only  $x$ - or  $y$ -polarized or both  $x$ - and  $y$ -polarized. The two transformations given by the fields (39) and (40) are both  $x$ - and  $y$ -polarized, which thus limits the number of transformations to  $\mathcal{N}(P) = P/4$ . If the transformation given by Eq. (40) was specified such that  $E_{iy,2} = 0$  (i.e. no polarization along  $y$ ), then this would release degrees of freedom and hence allow a triple transformation, i.e.  $\mathcal{N}(8) = 3 > 8/4$ . In addition, if the first transformation, given by Eq. (39), also had transverse components of the electric field polarized only along  $x$  or  $y$ , then we could achieve  $\mathcal{N}(8) = 4 > 8/4$  transformations. These considerations illustrate the necessity to perform educated selections in the metasurface synthesis procedure, as announced in Section 4.1.

#### 4.4 Metasurface with nonzero normal polarizations

Thus far, we have discarded the possibility of normal polarizations by enforcing  $P_z = M_z = 0$  in Eqs. (2)–(5). This is not only synthesis-wise convenient, as this suppresses the spatial derivatives in Eqs. (2)–(5), but also typically justified by the fact that any electromagnetic field can be produced by purely tangential surface currents/polarizations according to Huygens theorem. It was accordingly claimed in Ref. [103] that these normal polarizations, and corresponding susceptibility components, do not bring

<sup>16</sup> The synthesis technique yields the susceptibilities for an ideal zero-thickness metasurface. However, the metasurface sheet may be “approximated” by an electrically thin slab of thickness  $d$  ( $d \ll \lambda$ ) with volume susceptibility corresponding to a diluted version of the surface susceptibility, i.e.  $\chi_{\text{vol}} = \chi/d$  [80].

about any additional degrees of freedom and can thus be completely ignored. It turns out that this claim is generally not true: in fact,  $P_z$  and  $M_z$  provide extra degrees of freedom that allow a metasurface to perform a larger number of distinct operations for “different incident field configurations” and “at different times”.

Huygens theorem “exclusively” applies to a “single” (arbitrarily complex) combination of incident, reflected, and transmitted waves. This means that any metasurface, possibly involving normal polarizations, which performs the specified operation for such a single combination of fields, can be reduced to an equivalent metasurface with purely transverse polarizations. However, Huygens theorem does not apply to case of waves impinging on the metasurface at “different times”. Indeed, it is in this case impossible to superimpose the different incident waves to form a total incident field as they are not simultaneously illuminating the metasurface. Consequently, a purely tangential description of the metasurface is incomplete, and normal polarizations thus become necessary to perform the synthesis.

In fact, the presence of these normal susceptibility components greatly increases the number of degrees of freedom as the susceptibility tensors are now  $3 \times 3$  matrices instead of  $2 \times 2$  as in Eq. (16). This means that, for the four relevant GSTCs equations, we have now access to 36 unknown susceptibilities, instead of only 16, which increases the potential number of electromagnetic transformations from 4 to 9, provided that these transformations include fields that are independent from each other.

The synthesis of metasurfaces with nonzero normal polarization densities may be performed following similar procedures as those already discussed. As before, one needs to balance the number of unknown susceptibilities to the number of available equations provided by the GSTCs. Depending on the specifications, this may become difficult as many transformations may be required to obtain a full-rank system. Additionally, if the specified transformations involve changing the direction of wave propagation, then system (2)–(5) becomes a coupled system of partial differential equations in terms of the susceptibilities as the latter would now depend on the position. This generally prevents the derivation of closed-form solutions of the susceptibilities, which should rather be obtained numerically. However, we will now provide an example of a synthesis problem, where the susceptibilities are obtainable in closed form.

More specifically, we discuss the synthesis and analysis of a reciprocal metasurface with controllable angle-dependent scattering [104–106]. To synthesize this

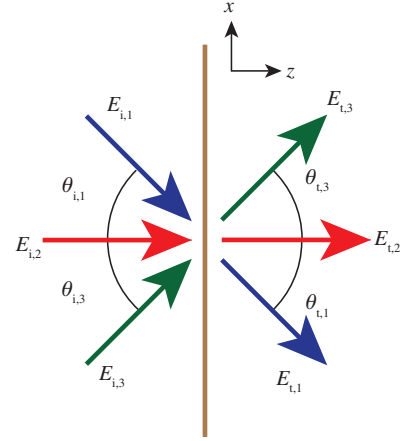


**Figure 6:** Multiple scattering from a uniform bianisotropic reflectionless metasurface.

metasurface, we consider the three “independent”<sup>17</sup> transformations depicted in Figure 6.

Specifying these three transformations allows one to achieve a relatively smooth control of the scattering response of the metasurface for any nonspecified incidence angles.

For simplicity, we specify that the metasurface does not change the direction of wave propagation, which implies that it is uniform, i.e. susceptibilities are not functions of position. Moreover, we specify that it is also reflectionless and only affects the transmission phase of p-polarized incident waves as function of their incidence angle.

To design this metasurface, we consider that it may be composed of a total number of 36 susceptibility components. However, as all the waves interacting with the metasurface are p-polarized, most of these susceptibilities will not be excited by these fields and thus will not play a role in the electromagnetic transformations. Accordingly, the only susceptibilities that are excited by the fields are

$$\bar{\bar{\chi}}_{ee} = \begin{pmatrix} \chi_{ee}^{xx} & 0 & \chi_{ee}^{xz} \\ 0 & 0 & 0 \\ \chi_{ee}^{zx} & 0 & \chi_{ee}^{zz} \end{pmatrix}, \quad \bar{\bar{\chi}}_{em} = \begin{pmatrix} 0 & \chi_{em}^{xy} & 0 \\ 0 & 0 & 0 \\ 0 & \chi_{em}^{zy} & 0 \end{pmatrix}, \quad (41)$$

$$\bar{\bar{\chi}}_{me} = \begin{pmatrix} 0 & 0 & 0 \\ \chi_{me}^{yx} & 0 & \chi_{me}^{yz} \\ 0 & 0 & 0 \end{pmatrix}, \quad \bar{\bar{\chi}}_{mm} = \begin{pmatrix} 0 & 0 & 0 \\ 0 & \chi_{mm}^{yy} & 0 \\ 0 & 0 & 0 \end{pmatrix}, \quad (42)$$

<sup>17</sup> It is essential to understand that these three sets of incident and transmitted waves “cannot” be combined, by superposition, into a single incident and a single transmitted wave because these waves are not necessarily impinging on the metasurface at the same time. This means that Huygens theorem cannot be used to find purely tangential equivalent surface currents corresponding to these fields.

where the susceptibilities not excited have been set to zero for simplicity. To satisfy the aforementioned specification of reciprocity, condition (12) must be satisfied. This implies that  $\chi_{ee}^{xz} = \chi_{ee}^{zx}$ ,  $\chi_{em}^{xy} = -\chi_{me}^{yx}$  and  $\chi_{em}^{zy} = -\chi_{me}^{yz}$ . As a consequence, the total number of independent susceptibility components in (41) and (42) reduces from 9 to 6.

Upon insertion of (41) and (42), the GSTCs in Eqs. (2) and (3) become

$$\Delta H_y = -j\omega\epsilon_0(\chi_{ee}^{xx}E_{x,av} + \chi_{ee}^{xz}E_{z,av}) - jk_0\chi_{em}^{xy}H_{y,av}, \quad (43)$$

$$\begin{aligned} \Delta E_x = & -j\omega\mu_0\chi_{mm}^{yy}H_{y,av} + jk_0(\chi_{em}^{xy}E_{x,av} + \chi_{em}^{zy}E_{z,av}) \\ & -\chi_{ee}^{xz}\partial_x E_{x,av} - \chi_{ee}^{zz}\partial_x E_{z,av} - \eta_0\chi_{em}^{zy}\partial_x H_{y,av}, \end{aligned} \quad (44)$$

where the spatial derivatives only apply to the fields and not to the susceptibilities as the latter are not functions space due to the uniformity of the metasurface.

System (43) and (44) contains two equations in six unknown susceptibilities and is thus underdetermined. To solve it, we apply the multiple transformation concept discussed in Section 4.3, which consists of specifying three independent sets of incident, reflected, and transmitted waves. These fields can be simply defined by their respective reflection ( $R$ )<sup>18</sup> and transmission ( $T$ ) coefficients as well as their incidence angle ( $\theta_i$ ). In our case, the metasurface exhibits a transmission phase shift,  $\phi$ , which is the function of the incidence angle, i.e.  $T = e^{j\phi(\theta_i)}$ .

Let us consider, for instance, that the three incident plane waves impinge on the metasurface at  $\theta_{i,1} = -45^\circ$ ,  $\theta_{i,2} = 0^\circ$ , and  $\theta_{i,3} = +45^\circ$  and are transmitted at  $\theta_t = \theta_i$  with transmission coefficients  $T_1 = e^{-j\alpha}$ ,  $T_2 = 1$ , and  $T_3 = e^{j\alpha}$ , where  $\alpha$  is a given phase shift. Solving relation (43) and (44) with these specifications yields the following nonzero susceptibilities:

$$\chi_{ee}^{xz} = \chi_{ee}^{zx} = \frac{2\sqrt{2}}{k_0} \tan\left(\frac{\alpha}{2}\right). \quad (45)$$

It can be easily verified that these susceptibilities satisfy the reciprocity, passivity, and losslessness conditions (13).

As susceptibility (45) corresponds to the only solution of system (43) and (44) for our specifications and as these susceptibilities correspond to the excitation of normal polarization densities, the normal polarizations are indeed useful and provide additional degrees of freedom. This proves the claim in the first paragraph of this section that normal polarizations lead to metasurface functionalities that are unattainable without them.

Now that the metasurface has been synthesized, we analyze its scattering response for all (including non-specified) incidence angles. For this purpose, we substitute susceptibility (45) into (43) and (44) and consider an incident wave, impinging on the metasurface at an angle  $\theta_i$ , being reflected and transmitted with unknown scattering parameters. System (43) and (44) can then be solved to obtain these unknown scattering parameters for any value of  $\theta_i$ . In our case, the analysis is simple because the metasurface is uniform, which means that the reflected and transmitted waves obey Snell laws. The resulting angular-dependent transmission coefficient is

$$T(\theta_i) = -1 + \frac{2}{1 - j\sqrt{2}\sin(\theta_i)\tan\left(\frac{\alpha}{2}\right)}, \quad (46)$$

while the reflection coefficient is  $R(\theta_i) = 0$ .

To illustrate the angular behavior of the transmission coefficient in Eq. (46), it is plotted in Figure 7 for a

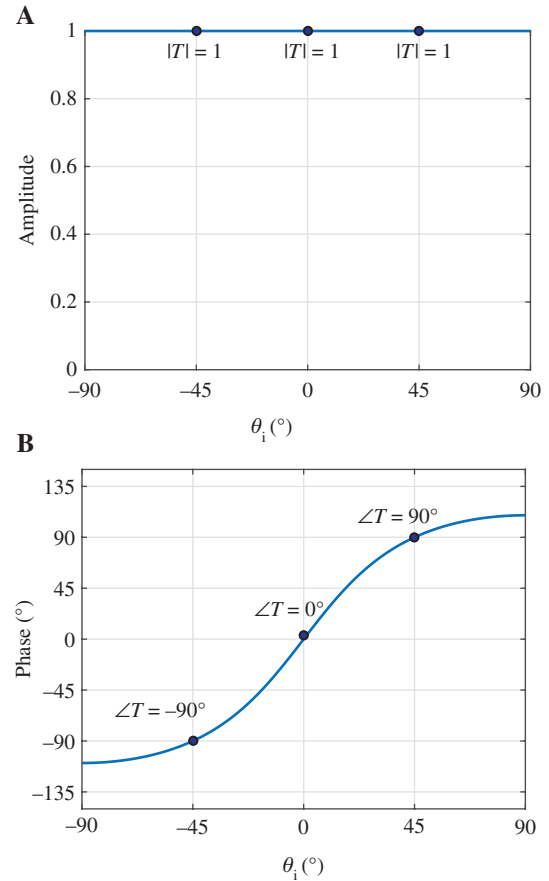


**Figure 7:** Transmission amplitude (A) and phase (B) as functions of the incidence angle for a metasurface synthesized for the transmission coefficients  $T = \{e^{-j90^\circ}; 1; e^{j90^\circ}\}$  (and  $R = 0$ ) at the respective incidence angles  $\theta_i = \{-45^\circ; 0^\circ; +45^\circ\}$ .

<sup>18</sup> Here,  $R = 0$  as the metasurface is reflectionless by specification.

specified phase shift of  $\alpha = 90^\circ$ . As expected, the transmission amplitude remains unity for all incidence angles, whereas the transmission phase is asymmetric around broadside and covers about a  $220^\circ$ -phase range.

#### 4.5 Relations with scattering parameters and implementation

We have seen how a metasurface can be synthesized to obtain its susceptibilities in terms of specified fields. We shall now investigate how the synthesized susceptibilities may be related to the shape of the scattering particles that will constitute the metasurfaces to be realized. Here, we will only present the mathematical expressions that relate the susceptibilities to the scattering particles. The reader is referred to [42, 83–90, 98, 107, 108] for more information on the practical realization of these structures.

The conventional method to relate the scattering particle shape to equivalent susceptibilities (or material parameters) is based on homogenization techniques. In the case of metamaterials, these techniques may be used to relate homogenized material parameters to the scattering parameters of the scatterers. From a general perspective, a single isolated scatterer is not sufficient to describe an homogenized medium. Instead, we shall rather consider a periodic array of scatterers, which takes into account the interactions and coupling between adjacent scatterers, hence leading to a more accurate description of a “medium” compared to a single scatterer. The susceptibilities, which describe the macroscopic responses of a medium, are thus naturally well-suited to describe the homogenized material parameters of metasurfaces. It follows that the equivalent susceptibilities of a scattering particle may be related to the corresponding scattering parameters, conventionally obtained via full-wave simulations, of a periodic array made of an infinite repetition of that scattering particle [83, 84, 109, 110].

Because the periodic array of scatterers is uniform with subwavelength periodicity, the scattered fields obey Snell laws. More specifically, if the incident wave propagates normally with respect to the array, then the reflected and transmitted waves also propagate normally. In most cases, the periodic array of scattering particles is excited with normally propagating waves. This allows one to obtain the 16 “tangential” susceptibility components in Eq. (37). However, it does not provide any information about the normal susceptibility components of the scattering particles. This is because, in the case of normally propagating waves, the normal susceptibilities do not induce any discontinuity of the fields, as explained in

Section 4.1. Nevertheless, this method allows one to match the tangential susceptibilities of the scattering particle to the susceptibilities found from the metasurface synthesis procedure and that precisely yields the ideal tangential susceptibility components.

It is clear that the scattering particles may, in addition to their tangential susceptibilities, possess nonzero normal susceptibility components. In that case, the scattering response of the metasurface, when illuminated with obliquely propagating waves, will differ from the expected ideal behavior prescribed in the synthesis. Consequently, the homogenization technique serves only as an initial guess to describe the scattering behavior of the metasurface.<sup>19</sup>

We will now derive the explicit expressions relating the tangential susceptibilities to the scattering parameters in the general case of a fully bianisotropic uniform metasurface surrounded by different media and excited by normally incident plane waves. Let us first write system (37) in the following compact form:

$$\bar{\bar{\Delta}} = \bar{\bar{\chi}} \cdot \bar{\bar{A}}_v, \quad (47)$$

where matrices  $\bar{\bar{\Delta}}$ ,  $\bar{\bar{\chi}}$  and  $\bar{\bar{A}}_v$  correspond to the field differences, the normalized susceptibilities, and the field averages, respectively.

To obtain the 16 tangential susceptibility components in Eq. (37), we will now define four transformations by specifying the fields on both sides of the metasurface. Let us consider that the metasurface is illuminated from the left with an  $x$ -polarized normally incident plane wave. The corresponding incident, reflected, and transmitted electric fields read

$$\mathbf{E}_i = \hat{\mathbf{x}}, \quad \mathbf{E}_r = S_{11}^{xx} \hat{\mathbf{x}} + S_{11}^{yx} \hat{\mathbf{y}}, \quad \mathbf{E}_t = S_{21}^{xx} \hat{\mathbf{x}} + S_{21}^{yx} \hat{\mathbf{y}}, \quad (48)$$

where the terms  $S_{ab}^{uv}$ , with  $a, b = \{1, 2\}$  and  $u, v = \{x, y\}$ , are the scattering parameters with ports 1 and 2 corresponding to the left and right sides of the metasurface, respectively, as shown in Figure 8.

The medium of the left of the metasurface has the intrinsic impedance  $\eta_1$ , whereas the medium on the right has the intrinsic impedance  $\eta_2$ . In addition to Eq. (48), three other cases have to be considered, i.e.  $y$ -polarized excitation incident from the left (port 1) and  $x$ - and  $y$ -polarized

<sup>19</sup> Note that it is possible to obtain all 36 susceptibility components of a scattering particle provided that the four GSTC relations are solved for nine independent sets of incident, reflected, and transmitted waves. In practice, such an operation is particularly tedious and is thus generally avoided.

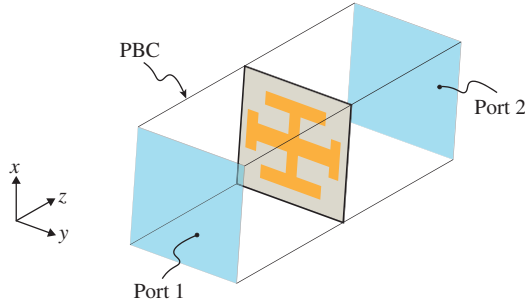


**Figure 8:** Full-wave simulation setup for the scattering parameter technique leading to the metasurface physical structure from the metasurface model based on Eq. (47). The unit cell is surrounded by PBCs and excited from ports 1 and 2.

excitations incident from the right (port 2). Inserting these fields into Eq. (37) leads, after simplification, to matrices  $\bar{\bar{\Delta}}$  and  $\bar{\bar{A}}_v$  given below:

$$\bar{\bar{\Delta}} = \begin{pmatrix} -\bar{N}_2/\eta_1 + \bar{N}_2 \cdot \bar{S}_{11}/\eta_1 + \bar{N}_2 \cdot \bar{S}_{21}/\eta_2 & -\bar{N}_2/\eta_2 + \bar{N}_2 \cdot \bar{S}_{12}/\eta_1 + \bar{N}_2 \cdot \bar{S}_{22}/\eta_2 \\ -\bar{N}_1 \cdot \bar{N}_2 - \bar{N}_1 \cdot \bar{N}_2 \cdot \bar{S}_{11} + \bar{N}_1 \cdot \bar{N}_2 \cdot \bar{S}_{21} & \bar{N}_1 \cdot \bar{N}_2 - \bar{N}_1 \cdot \bar{N}_2 \cdot \bar{S}_{12} + \bar{N}_1 \cdot \bar{N}_2 \cdot \bar{S}_{22} \end{pmatrix}, \quad (49)$$

$$\bar{\bar{A}}_v = \frac{1}{2} \begin{pmatrix} \bar{I} + \bar{S}_{11} + \bar{S}_{21} & \bar{I} + \bar{S}_{12} + \bar{S}_{22} \\ \bar{N}_1/\eta_1 - \bar{N}_1 \cdot \bar{S}_{11}/\eta_1 + \bar{N}_1 \cdot \bar{S}_{21}/\eta_2 & -\bar{N}_1/\eta_2 - \bar{N}_1 \cdot \bar{S}_{12}/\eta_1 + \bar{N}_1 \cdot \bar{S}_{22}/\eta_2 \end{pmatrix}. \quad (50)$$

where the matrices  $\bar{S}_{ab}$ ,  $\bar{I}$ ,  $\bar{N}_1$  and  $\bar{N}_2$  are defined by

$$\bar{S}_{ab} = \begin{pmatrix} S_{ab}^{xx} & S_{ab}^{xy} \\ S_{ab}^{yx} & S_{ab}^{yy} \end{pmatrix}, \quad \bar{I} = \begin{pmatrix} 1 & 0 \\ 0 & 1 \end{pmatrix}, \quad (51)$$

$$\bar{N}_1 = \begin{pmatrix} 0 & -1 \\ 1 & 0 \end{pmatrix}, \quad \bar{N}_2 = \begin{pmatrix} 1 & 0 \\ 0 & -1 \end{pmatrix}.$$

Now, the procedure to obtain the susceptibilities of a given scattering particle is as follows: first, the scattering particle is simulated with periodic boundary conditions (PBCs) and normal excitation. Second, the resulting scattering parameters obtained from the simulations are used to define the matrices in Eqs. (49) and (50). Finally, the susceptibilities corresponding to the particle are obtained by matrix inversion of Eq. (47).

Alternatively, it is possible to obtain the scattering parameters of a normally incident plane being scattered by a uniform metasurface with known susceptibilities [111]. This can be achieved by solving Eq. (47) for the scattering parameters. This leads to the following matrix equation:

$$\bar{\bar{S}} = \bar{\bar{M}}_1^{-1} \cdot \bar{\bar{M}}_2, \quad (52)$$

where the scattering parameter matrix,  $\bar{\bar{S}}$ , is defined as

$$\bar{\bar{S}} = \begin{pmatrix} \bar{S}_{11} & \bar{S}_{12} \\ \bar{S}_{21} & \bar{S}_{22} \end{pmatrix}, \quad (53)$$

and matrices  $\bar{\bar{M}}_1$  and  $\bar{\bar{M}}_2$  are obtained from Eqs. (47), (49), and (50) by expressing the scattering parameters in terms of the normalized susceptibility tensors. The resulting matrices  $\bar{\bar{M}}_1$  and  $\bar{\bar{M}}_2$  are given below:

$$\bar{\bar{M}}_1 = \begin{pmatrix} \bar{N}_2/\eta_1 - \hat{\chi}_{ee}/2 + \hat{\chi}_{em} \cdot \bar{N}_1/(2\eta_1) & \bar{N}_2/\eta_2 - \hat{\chi}_{ee}/2 - \hat{\chi}_{em} \cdot \bar{N}_1/(2\eta_2) \\ -\bar{N}_1 \cdot \bar{N}_2 - \hat{\chi}_{me}/2 + \hat{\chi}_{mm} \cdot \bar{N}_1/(2\eta_1) & \bar{N}_1 \cdot \bar{N}_2 - \hat{\chi}_{me}/2 - \hat{\chi}_{mm} \cdot \bar{N}_1/(2\eta_2) \end{pmatrix}, \quad (54)$$

$$\bar{\bar{M}}_2 = \begin{pmatrix} \hat{\chi}_{ee}/2 + \bar{N}_2/\eta_1 + \hat{\chi}_{em} \cdot \bar{N}_1/(2\eta_1) & \hat{\chi}_{ee}/2 + \bar{N}_2/\eta_2 - \hat{\chi}_{em} \cdot \bar{N}_1/(2\eta_2) \\ \hat{\chi}_{me}/2 + \bar{N}_1 \cdot \bar{N}_2 + \hat{\chi}_{mm} \cdot \bar{N}_1/(2\eta_1) & \hat{\chi}_{me}/2 - \bar{N}_1 \cdot \bar{N}_2 - \hat{\chi}_{mm} \cdot \bar{N}_1/(2\eta_2) \end{pmatrix}. \quad (55)$$

Thus, the final metasurface physical structure is obtained by mapping the scattering parameters (53) obtained from the discretized synthesized susceptibilities by Eq. (52) via Eqs. (54) and (55) to those obtained by full-wave simulating metasurface unit cells with tunable parameters, in an approximate periodic environment, as illustrated in Figure 8. Unfortunately, there is currently no straightforward method to relate the susceptibilities found from the synthesis to the specific geometry of the scattering particles and one therefore has to strongly rely on numerical simulations and optimizations in that step of the synthesis. Note that group theory has been proposed as a potential mathematical tool to relate the geometry of the scattering particles to their effective susceptibilities [112–114]. However, this approach has not been widely used thus far, and less elegant but still quite efficient empirical approaches are preferred at this point.

A typical unit cell structure allowing arbitrary designs, at least at microwave frequencies, is a stack of three metallic layers separated by dielectric spacers [86, 115–117]. In this structure, the metallic layers may for instance take the shape of Jerusalem crosses similar to that depicted in Figure 8. The advantage of this geometry is that the  $x$ - and  $y$ -polarizations may be almost independently controlled by varying the dimensions of the arms of the crosses.

The unit cell may be longitudinally symmetric (same outer layers) or asymmetric. In the symmetric case, the two lowest resonant modes of the entire structure may be decomposed into even and odd modes, which

respectively correspond to electric and magnetic dipolar resonances. Controlling the overall response of the unit cell is thus achieved by tuning its electric and magnetic responses, which leads to different values of the susceptibilities. Due to symmetry, the magnetic response is controlled by changing only the two outer layers as, for the odd mode, there is no current flowing on the middle layer. In contrast, the geometry of the three layers affects the electric response. Accordingly, the general procedure to implement a unit cell so that it exhibits the susceptibilities obtained from the synthesis is as follows: first, the magnetic susceptibility is obtained by changing the geometry of the unit cell outer layers. Then, the electric susceptibility is obtained by changing the geometry of the remaining middle layer. If the unit cell is asymmetric, then the two lowest resonances cannot split into even and an odd modes as they are now coupled to each other. Due to this asymmetry, and resulting mode coupling, the unit cell exhibits more degrees of freedom, which incidentally allows one to implement bianisotropic metasurfaces.

Implementing unit cell structures made of three metallic layers is also possible at optical frequencies [83]. However, such structures are practically difficult to realize using current fabrication processes. A more practical optical unit cell structure would be one based on dielectric resonators [118–120]. Such resonators, which naturally possess electric and magnetic resonances, typically have a cylindrical or elliptical cross-section for isotropic or anisotropic field control, respectively. Their design is much simpler than that of the three-layer structures, as their responses are generally controlled by tuning only the radius for the cylindrical ones and the ellipticity and orientation for the elliptical ones.

Due to the subwavelength unit cell period of metasurfaces, coupling between the scattering particles is unavoidable. However, strong coupling is not necessarily detrimental. Indeed, it may help reducing the overall unit cell size via increased field interactions and it may also be leveraged to increase the bandwidth of the structure [121].

In cases where coupling would be detrimental, it is practically difficult to address it otherwise than resorting to brute-force numerical optimization tools of full-wave simulation software. Nevertheless, in the case of spatially varying metasurfaces, it is possible to reduce the detrimental effects of coupling by ensuring slow spatial variations compared to the unit cell size. Then, the scattering particles of adjacent unit cells are almost identical to each other, meaning that the coupling between them is also almost identical to that when they were initially simulated in a perfectly periodic environment. This greatly simplifies the realization of spatially varying metasurfaces as their implementation becomes much less cumbersome.

## 5 Concepts and applications

In the previous section, we have shown several metasurface examples as “illustrations” of the proposed synthesis technique. These examples did not necessarily correspond to practical designs but, in addition to illustrating the proposed synthesis technique, they did set up the stage for the development of useful and practical concepts and applications, which is the object of the present section.

We shall present here five of our most recent works representing novel concepts and applications of metasurfaces. In the order of appearance, we present our work on birefringent transformations [98, 122], bianisotropic refraction [123], light emission enhancement [124], remote spatial processing [125], and nonlinear second-harmonic generation (SHG) [96]. The reader is also referred to our related works on nonreciprocal nongyrotropic isolators [126], dielectric metasurfaces for dispersion engineering [127], and radiation pressure control [128].

### 5.1 Birefringent operations

A direct application of the synthesis procedure discussed in Section 4, and more specifically of the susceptibilities in (19) and (20), is the design of birefringent metasurfaces. These susceptibilities are split into two independent sets that allow to individually control the scattering of s- and p-polarized waves. In particular, the manipulation of the respective transmission phases of these orthogonal waves allows several interesting operations.

In Ref. [122], we have used this approach to realize half-wave plates, which rotate the polarization of linearly polarized waves by  $90^\circ$  or invert the handedness of circularly polarized waves, quarter-wave plates that convert linear polarization into circular polarization, a polarization beam splitter that spatially separates orthogonally polarized waves, and an orbital angular momentum generator that generates topological charges that depend on the incident wave polarization. These operations are depicted in Figure 9.

### 5.2 “Perfect” refraction

Most refractive operations realized thus far with a metasurface have been based on the concept of the generalized law of refraction [43], which requires the implementation of a phase gradient structure. However, such structures are plagued by undesired diffraction orders and are thus not

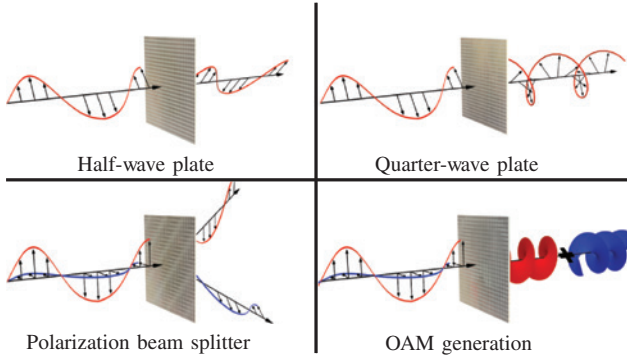


**Figure 9:** Birefringent metasurface transformations presented in Ref. [122].

fully efficient. It turns out that the fundamental reason for this efficiency limitation is the symmetric nature of simple (early as in Ref. [43]) refractive metasurfaces with respect to the  $z$ -direction. This can be demonstrated by the following *ad absurdum* argument.

Let us consider a passive metasurface surrounded by a given reciprocal<sup>20</sup> medium and denote the two sides of the structure by indices 1 and 2. Assume that this metasurface “perfectly” refracts (without reflection and spurious diffraction) a wave incident under the angle  $\theta_1$  in side 1 to the angle  $\theta_2$  in side 2, and assume, *ad absurdum*, that this metasurface is “symmetric” with respect to its normal. As it is reciprocally perfectly refracting, it is perfectly matched for both propagation directions: 1-2 and 2-1. Consider first wave propagation from side 1 to side 2. Due to perfect matching, the wave experiences no reflection and, due to perfect refraction, it is fully transmitted to the angle  $\theta_2$  in side 2. Consider now wave propagation in the opposite direction along the reciprocal (or time-reversed) path. Now, the wave incident in side 2 has different tangential field components than that incident in side 1, assuming  $\theta_2 \neq \theta_1$ ; therefore, it will see a different impedance, which means that the metasurface is necessarily mismatched in the direction 2-1. However, this is in contradiction with the assumption of perfect (reciprocal) refraction. Consequently, the symmetric metasurface does not produce perfect refraction. Part of the wave incident from side 2 is reflected back; therefore, by reciprocity, matching also did not actually exist in the direction 1-2, so all of the energy of the wave incident under  $\theta_1$  in side 1 cannot completely refract into  $\theta_2$ ; part of it has to be

<sup>20</sup> The quasi-totality of the refracting metasurfaces discussed in the literature thus far has been reciprocal. The following argument does not hold for the nonreciprocal case, where perfect refraction could in principle be achieved by a symmetric metasurface structure.

transmitted to other directions in side 2, which typically represents spurious diffraction orders assuming a periodic-gradient metasurface. These diffraction orders are consistently visible in reported simulations and experiments of symmetric metasurfaces intended to perform refraction.

It was demonstrated in Refs. [116, 123] that “bianisotropy” was the solution to realize perfect (reciprocal) refraction (100% power transmission efficiency from  $\theta_1$  to  $\theta_2$ ). In what follows, we summarize the main synthesis steps for such a metasurface.

Let us consider the bianisotropic GSTC relations in Eq. (16). For a refractive metasurface, the rotation of polarization is not required and usually undesired. Therefore, the relevant nonzero susceptibility components reduce to the diagonal components of  $\tilde{\chi}_{ee}$  and  $\tilde{\chi}_{mm}$  and the off-diagonal components of  $\tilde{\chi}_{em}$  and  $\tilde{\chi}_{me}$ . This corresponds to  $4 \times 2 = 8$  susceptibility parameters, leading, according to Section 4.3, to the double-transformation full-rank system

$$\begin{pmatrix} \Delta H_{y1} & \Delta H_{y2} \\ \Delta H_{x1} & \Delta H_{x2} \\ \Delta E_{y1} & \Delta E_{y2} \\ \Delta E_{x1} & \Delta E_{x2} \end{pmatrix} = \begin{pmatrix} \tilde{\chi}_{ee}^{xx} & 0 & 0 & \tilde{\chi}_{em}^{xy} \\ 0 & \tilde{\chi}_{ee}^{yy} & \tilde{\chi}_{em}^{yx} & 0 \\ 0 & \tilde{\chi}_{me}^{xy} & \tilde{\chi}_{mm}^{xx} & 0 \\ \tilde{\chi}_{me}^{yx} & 0 & 0 & \tilde{\chi}_{mm}^{yy} \end{pmatrix} \begin{pmatrix} E_{x1,av} & E_{x2,av} \\ E_{y1,av} & E_{y2,av} \\ H_{x1,av} & H_{x2,av} \\ H_{y1,av} & H_{y2,av} \end{pmatrix}, \quad (56)$$

where we naturally specify the second transformation as the reciprocal of the first one. Assuming that the refraction takes places in the  $xz$ -plane and that the waves are all  $p$ -polarized, system (56) reduces to

$$\begin{pmatrix} \Delta H_{y1} & \Delta H_{y2} \\ \Delta E_{x1} & \Delta E_{x2} \end{pmatrix} = \begin{pmatrix} \tilde{\chi}_{ee}^{xx} & \tilde{\chi}_{em}^{xy} \\ \tilde{\chi}_{me}^{yx} & \tilde{\chi}_{mm}^{yy} \end{pmatrix} \begin{pmatrix} E_{x1,av} & E_{x2,av} \\ H_{y1,av} & H_{y2,av} \end{pmatrix}, \quad (57)$$

which strictly corresponds to a system that is  $\mathcal{N}(4) = 2$ , although the initial goal might have been to perform refraction in one propagation direction only. An illustration of the first and second transformations is presented in Figure 10A and B, respectively. Note that subscripts  $i$  and  $t$ , respectively, refer to the incident and transmit sides of the metasurface rather than the incident and transmitted waves.

The electromagnetic fields on the incident and transmit sides of the metasurface, assuming that the media on

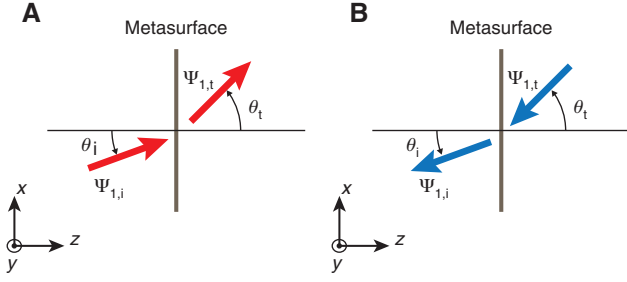


**Figure 10:** Representation of the two transformations specified in system (57): (A) first transformation corresponding to the fields in (58) and (59) and (B) second transformation corresponding to the fields in (60) and (61).

both sides are vacuum and that correspond to the first transformation, read

$$E_{x1,i} = \frac{k_{z,i}}{k_0} e^{-jk_{x,i}x}, \quad E_{x1,t} = A_t \frac{k_{z,t}}{k_0} e^{-jk_{x,t}x}, \quad (58)$$

$$H_{y1,i} = e^{-jk_{x,i}x} / \eta_0, \quad H_{y1,t} = A_t e^{-jk_{x,t}x} / \eta_0, \quad (59)$$

where  $A_t$  is the amplitude of the wave on the transmit side. The fields corresponding to the second transformation read

$$E_{x2,i} = -\frac{k_{z,i}}{k_0} e^{jk_{x,i}x}, \quad E_{x2,t} = -A_t \frac{k_{z,t}}{k_0} e^{jk_{x,t}x}, \quad (60)$$

$$H_{y2,i} = e^{jk_{x,i}x} / \eta_0, \quad H_{y2,t} = A_t e^{jk_{x,t}x} / \eta_0. \quad (61)$$

To ensure power conservation between the incident and transmitted waves, the amplitude of the transmitted wave must be  $A_t = \sqrt{k_{z,i} / k_{z,t}} = \sqrt{\cos\theta_i / \cos\theta_t}$ , as shown in Ref. [123]. Under this condition, the metasurface susceptibilities, obtained by substituting (58), (59) and (60), (61) into (57) and considering the normalization (17), read

$$\chi_{ee}^{xx} = \frac{4\sin(\alpha x)}{\beta \cos(\alpha x) + \sqrt{\beta^2 - \gamma^2}}, \quad (62)$$

$$\chi_{mm}^{yy} = \frac{\beta^2 - \gamma^2}{4k_0^2} \frac{4\sin(\alpha x)}{\beta \cos(\alpha x) + \sqrt{\beta^2 - \gamma^2}}, \quad (63)$$

$$\chi_{em}^{xy} = -\chi_{me}^{yx} = \frac{2j}{k_0} \frac{\gamma \cos(\alpha x)}{\beta \cos(\alpha x) + \sqrt{\beta^2 - \gamma^2}}, \quad (64)$$

where  $\alpha = k_{x,t} - k_{x,i}$ ,  $\beta = k_{z,i} + k_{z,t}$ , and  $\gamma = k_{z,i} - k_{z,t}$ . It can be easily verified, using Eq. (13), that the bianisotropic

refractive metasurface with susceptibility (62)–(64) corresponds to a reciprocal, passive, and lossless structure, in addition to being immune to reflection and spurious diffraction, and is hence a perfectly refractive metasurface.

To demonstrate the performance of the synthesis method, we have built two bianisotropic refractive metasurfaces [123]. They respectively transform an incident wave impinging at  $\theta_i = 20^\circ$  into a transmitted wave refracted at  $\theta_t = -28^\circ$  and a normally incident wave into a transmitted wave refracted at  $\theta_t = -70^\circ$ . The full-wave simulations corresponding to these transformations are plotted in Figure 11A and B, respectively. The simulated power transmission of these two structures is 86.7% and 83.2%, respectively. These efficiencies are mostly limited to the inherent dielectric and metallic losses of the scattering particles and, to a lesser extent, to the undesired diffraction orders due to the imperfection of these particles. A corresponding metasurface was demonstrated in Ref. [123] with an efficiency (79%) that is approximately 4% superior to the theoretical limit of a “lossless” monoanisotropic metasurface, hence unquestionably demonstrating the superiority of the bianisotropic design.

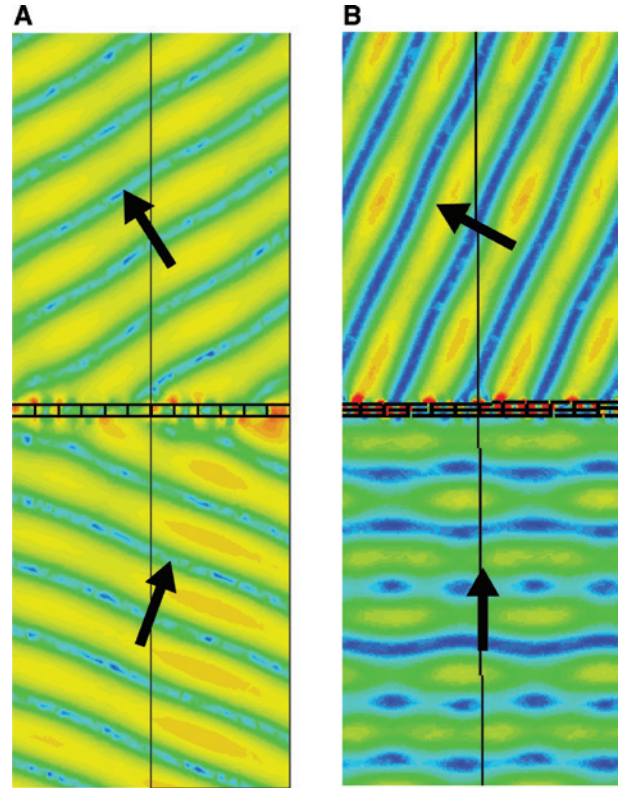


**Figure 11:** Full-wave simulations showing the performance of two refractive metasurfaces [123].

### 5.3 Remote spatial processing

Metasurface remote spatial processing, introduced in Ref. [125], consists of controlling the transmission of a signal beam through a metasurface by remotely sending a control beam, which properly interferes with the signal beam. This interference is thus used to shape the metasurface transmission pattern by varying the phase and/or amplitude of the control beam.

Figure 12 presents an example of such remote spatial processing. Initially, the signal beam (in blue) in Figure 2A is refracted by the metasurface according to some initial specification. When the control beam (in red) is next added to the signal beam on the metasurface, as in Figure 12B, it changes the overall radiation pattern of the metasurface.

We have used this concept to implement remote spatial switch/modulators. The operation principle of such a modulator is presented in Figure 13. To avoid the collocation of the control and signal beam sources, the control beam impinges on the metasurface at an angle while the signal beam is normally incident. To independently control the transmission of both beams, they must be orthogonally polarized on the incident side of the metasurface. However, they must exhibit the same polarization on the transmit side to interfere. In Ref. [125], we show that such a transformation can only be achieved using a bianisotropic metasurface, which must also be chiral to rotate the polarization of the control beam. On the transmit side, the two beams interfere and the corresponding amplitude thus depends of the phase difference between them.

The fabricated metasurface performing the operation depicted in Figure 13 has been experimentally measured, and the corresponding results are plotted in Figure 14 for an operating frequency of 16 GHz.

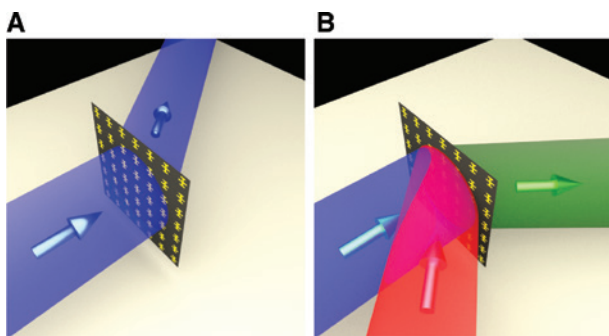


**Figure 12:** Example of a remote spatial processing operation: (A) signal beam being refracted by the metasurface and (B) superposition of signal and control beams interacting with each other, which leads to a different transmitted wave.

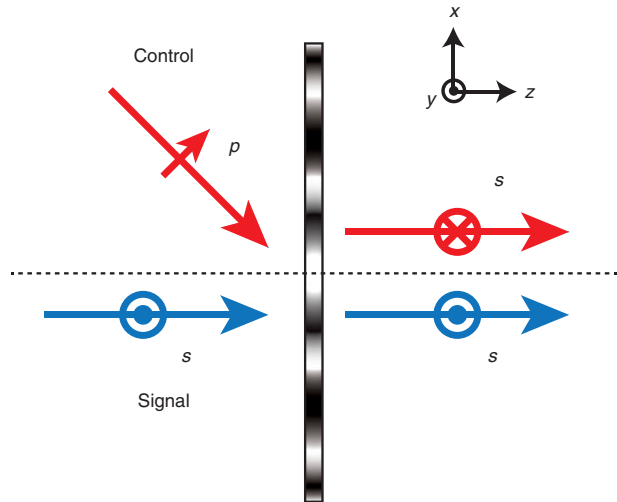


**Figure 13:** Coherent modulator metasurface.

The signal and control beams are impinging on the metasurface at different angles to avoid collocation of their source. The amplitude of the transmitted wave depends on the phase difference between the two beams by interference.

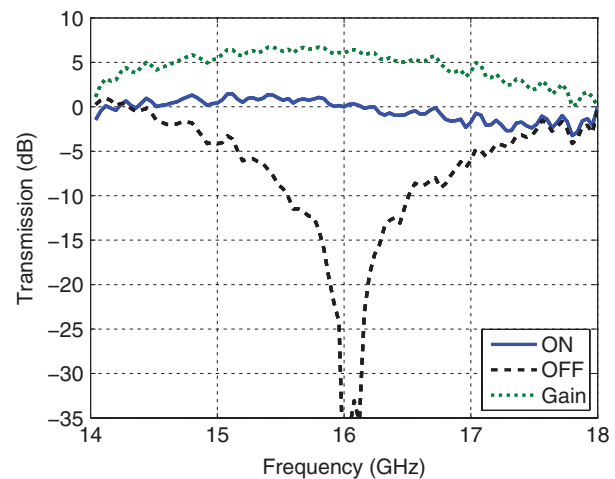


**Figure 14:** Measured transmission coefficients for the metasurface in Figure 13.

The blue curve is the transmission of the signal beam only, whereas the black and green curves are the destructive and constructive interferences of the signal and control beams, respectively.

### 5.4 Light emission enhancement

In the perspective of enhancing the efficiency of light-emitting diodes (LEDs), we have reported in Ref. [124] a partially reflecting metasurface cavity (PRMC) increasing the emission of photon sources in layered semiconductor structures using the susceptibility-GSTC technique presented in this paper. This PRMC simultaneously enhances the light extraction efficiency (LEE), spontaneous

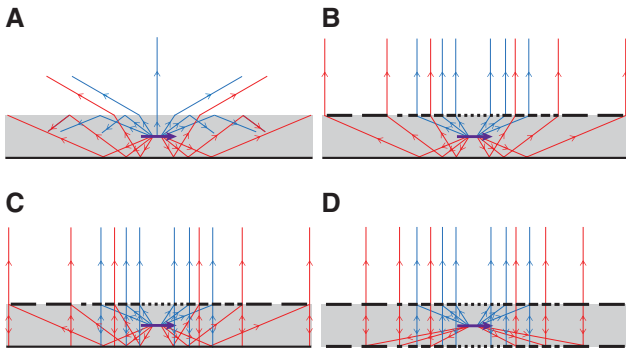
emission rate (SER), and far-field directivity of the photon source.

The LEE is enhanced by enforcing the emitted light to optimally refract/radiate perpendicularly to the device. Such refraction suppresses the wave trapping loss, as represented in Figure 15A. The requirement of total normal refraction, as represented in Figure 15B, is excessively stringent, leading to susceptibilities with prohibitive spatial variations, and is not required in this application. A better strategy consists, as illustrated in Figure 15C, in allowing partial local reflection and ultimately collecting the reflected part of the energy by Fabry-Perot resonance in the PRMC formed with a mirror plane at the bottom of the slab. The double-metasurface cavity, as depicted in Figure 15D, is an even more sophisticated design, leading to dramatic LEE enhancement.

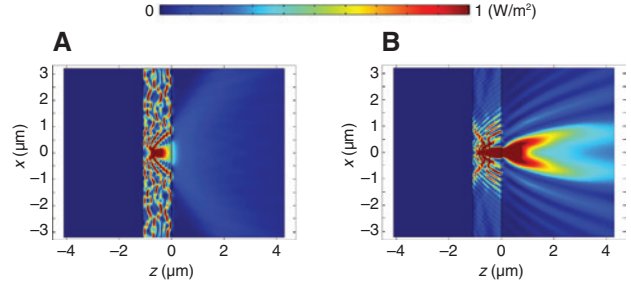
The SER is enhanced by maximizing the confinement of coherent electromagnetic energy in the vicinity of the source and leveraging the Purcell effect, which is particularly well achieved in the double-metasurface PRMC (Figure 15D). Finally, the far-field directivity is maximized as an optimization tradeoff for maximal overall power conversion ratio.

Figure 16 shows the full-wave simulated flux densities for the designs of Figure 15A and D, where the latter features LEE and SER enhancements by factors of 4.0 and 1.9, respectively, with half-power beam width of  $22.5^\circ$ .

The case of a real LED is more complex due to the incoherence and distribution emission of the quantum well emitters. Different metasurface strategies are currently being investigated to maximize the power conversion efficiency of a complete LED.



**Figure 15:** Radiation of a light source (quantum well) embedded in a semiconductor (e.g. GaN) substrate: (A) bare structure; (B) reflectionless metasurface, placed on top of the slab, which collimates the dipole fields; (C) introduction of PRMC; and (D) double-metasurface cavity, with partially reflective top metasurface and fully reflective bottom metasurface.



**Figure 16:** Full-wave (COMSOL) simulated energy flux densities for a dipole emitter embedded in a GaN slab: (A) configuration of Figure 15A and (B) configuration of Figure 15D. Original images from Ref. [124].

## 5.5 Second-order nonlinearity

Thus far, we have only discussed linear metasurfaces, i.e. metasurfaces whose polarization densities are linear functions of the electric and magnetic fields. Given the wealth of potential applications of nonlinear metasurfaces, it is highly desirable to develop tools for the design of such metasurfaces. Therefore, we extended our susceptibility-GSTC technique to the case of a second-order nonlinear metasurface in Ref. [96].

In this case, the polarization densities can be written as

$$\mathbf{P} = \epsilon_0 \overline{\overline{\chi}}_{ee}^{(1)} \cdot \mathbf{E}_{av} + \epsilon_0 \overline{\overline{\chi}}_{ee}^{(2)} : \mathbf{E}_{av} \mathbf{E}_{av}, \quad (65)$$

$$\mathbf{M} = \overline{\overline{\chi}}_{mm}^{(1)} \cdot \mathbf{H}_{av} + \overline{\overline{\chi}}_{mm}^{(2)} : \mathbf{H}_{av} \mathbf{H}_{av}, \quad (66)$$

where  $\overline{\overline{\chi}}^{(1)}$  and  $\overline{\overline{\chi}}^{(2)}$  are to the linear and nonlinear (second-order) susceptibilities of the metasurface. For the sake of simplicity, we assume that these susceptibility tensors are scalar. Being nonlinear, the metasurface will generate harmonics of the excitation frequency  $\omega_0$ . Consequently, we have to express the GSTCs in Eqs. (2)–(5) in the time-domain to properly take into account the generation of these new frequencies. The relevant GSTCs are then, in the case of  $x$ -polarized waves, given by<sup>21</sup>

$$-\Delta H = \epsilon_0 \chi_{ee}^{(1)} \frac{\partial}{\partial t} E_{av} + \epsilon_0 \chi_{ee}^{(2)} \frac{\partial}{\partial t} E_{av}^2, \quad (67)$$

$$-\Delta E = \mu_0 \chi_{mm}^{(1)} \frac{\partial}{\partial t} H_{av} + \mu_0 \chi_{mm}^{(2)} \frac{\partial}{\partial t} H_{av}^2, \quad (68)$$

<sup>21</sup> In these expressions, the susceptibilities are dispersion less. Meaning that  $\chi(\omega_0) = \chi(2\omega_0) = \chi(3\omega_0) = \dots$ , as discussed in Ref. [96], which is essentially equivalent to the conventional condition of phase-matching in nonlinear optics.

where  $E$  and  $H$  are the  $x$ -component of the electric field and the  $y$ -component of the magnetic field, respectively. From these relations, we can either perform a synthesis, i.e. expressing the susceptibilities as functions of the fields, or an analysis, i.e. computing the fields scattered from a metasurface with known susceptibilities. Here, for the sake of brevity, we will not elaborate on the synthesis and analysis operations but shall rather present one of the main results obtained in Ref. [96], which are the reflectionless conditions for the metasurface. The metasurface with susceptibility (67) and (68) exhibit different reflectionless conditions for the two propagation directions as, due to the presence of the square of both the electric and magnetic fields, relation (67) and (68) is asymmetric with respect to the  $z$ -direction. It follows that the reflectionless conditions for waves propagating in the forward (+ $z$ ) direction are

$$\chi_{ee}^{(1)} = \chi_{mm}^{(1)}, \quad (69)$$

$$\eta_0 \chi_{ee}^{(2)} = \chi_{mm}^{(2)}, \quad (70)$$

whereas for backward (- $z$ ) propagation they are

$$\chi_{ee}^{(1)} = \chi_{mm}^{(1)}, \quad (71)$$

$$-\eta_0 \chi_{ee}^{(2)} = \chi_{mm}^{(2)}. \quad (72)$$

An important consequence of the fact that the metasurface cannot be matched from both sides is that its SHG is inherently nonreciprocal.

## 6 Conclusions

We have presented an overview of electromagnetic metasurface designs, concepts, and applications based on a bianisotropic surface susceptibility tensor model. This overview probably represents only a small fraction of this approach, which nevertheless already represents a solid foundation for future metasurface technology.

**Acknowledgments:** This work was accomplished in the framework of the Collaborative Research and Development Project (CRDPJ 478303-14) of the Natural Sciences and Engineering Research Council of Canada in partnership with Metamaterial Technology, Inc.

## References

- [1] Holloway C, Dienstfrey A, Kuester EF, O'Hara JF, Azad AK, Taylor AJ. A discussion on the interpretation and characterization of

metafilms/metamaterials: the two-dimensional equivalent of metamaterials. *Metamaterials* 2009;3:100–12.

- [2] Holloway C, Kuester EF, Gordon J, O'Hara J, Booth J, Smith D. An overview of the theory and applications of metasurfaces: the two-dimensional equivalents of metamaterials. *IEEE Antennas Propag Mag* 2012;54:10–35.
- [3] Minovich AE, Miroshnichenko AE, Bykov AY, Murzina TV, Neshev DN, Kivshar YS. Functional and nonlinear optical metasurfaces. *Laser Photon Rev* 2015;9:195–213.
- [4] Glybovski SB, Tretyakov SA, Belov PA, Kivshar YS, Simovski CR. Metasurfaces: from microwaves to visible. *Phys Rep* 2016;634:1–72.
- [5] Kildishev AV, Boltasseva A, Shalaev VM. Planar photonics with metasurfaces. *Science* 2013;339:1232009. doi: 10.1126/science.1232009.
- [6] Lamb H. On the reflection and transmission of electric waves by a metallic grating. *Proc Lond Math Soc* 1897;1:523–46.
- [7] Marconi G, Franklin C. Reflector for use in wireless telegraphy and telephony. April 22 1919, US Patent 1,301,473.
- [8] Buskirk LV, Hendrix C. The zone plate as a radio-frequency focusing element. *IRE Trans Antennas Propag* 1961;9:319–20.
- [9] Munk BA. *Frequency Selective surfaces: theory and design*. Chichester, UK, John Wiley & Sons, 2000.
- [10] Rashid AK, Li B, Shen Z. An overview of three-dimensional frequency-selective structures. *IEEE Antennas Propag Mag* 2014;56:43–67.
- [11] Huang J, Encinar JA. *Reflectarray antenna*. Chichester, UK, Wiley Online Library, 2007.
- [12] Berry D, Malech R, Kennedy W. The reflectarray antenna. *IEEE Trans Antennas Propag* 1963;11:645–51.
- [13] Malagisi C. Microstrip disc element reflect array. In: *EASCON'78: Electronics and Aerospace Systems Convention* 1978:186–92.
- [14] Montgomery JP. A microstrip reflectarray antenna element. *Antenna Applications Symposium, University of Illinois*, 1978.
- [15] Stangel J. The thinned lens approach to phased array design. In: *1965 Antennas and Propagation Society International Symposium* 1965:10–3.
- [16] Kahrilas PJ. Hapdar 8212: an operational phased array radar. *Proc IEEE* 1968;56:1967–75.
- [17] McGrath D. Planar three-dimensional constrained lenses. *IEEE Trans Antennas Propag* 1986;34:46–50.
- [18] Pozar DM. Flat lens antenna concept using aperture coupled microstrip patches. *Electron Lett* 1996;32:2109–11.
- [19] Lam K-W, Kwok S-W, Hwang Y, Lo TK. Implementation of transmitarray antenna concept by using aperture-coupled microstrip patches. In: *Proceedings of 1997 Asia-Pacific Microwave Conference* 1997;1:433–6.
- [20] Datthanasombat S, Prata A, Arnaro LR, Harrell JA, Spitz S, Perret J. Layered lens antennas. In: *IEEE Antennas and Propagation Society International Symposium, 2001 Digest, held in conjunction with: USNC/URSI National Radio Science Meeting (Cat. No. 01CH37229)* 2001;2:777–80.
- [21] Gagnon N, Petosa A, McNamara D. Thin microwave quasi-transparent phase-shifting surface (PSS). *IEEE Trans Antennas Propag* 2010;58:1193–201.
- [22] Imani MF, Grbic A. An analytical investigation of near-field plates. *Metamaterials* 2010;4:104–11.
- [23] Grbic A, Jiang L, Merlin R. Near-field plates: subdiffraction focusing with patterned surfaces. *Science* 2008;320:511–3.
- [24] Imani M, Grbic A. Planar near-field plates. *IEEE Trans Antennas Propag* 2013;61:5425–34.

- [25] Fong B, Colburn J, Ottusch J, Visher J, Sievenpiper D. Scalar and tensor holographic artificial impedance surfaces. *IEEE Trans Antennas Propag* 2010;58:3212–21.
- [26] Maci S, Minatti G, Casaletti M, Bosiljevac M. Metasurfing: addressing waves on impenetrable metasurfaces. *IEEE Antennas Wireless Propag Lett* 2011;10:1499–502.
- [27] Song K, Zhao X, Liu Y, Fu Q, Luo C. A frequency-tunable 90°-polarization rotation device using composite chiral metamaterials. *Appl Phys Lett* 2013;103:101908.
- [28] Martinez-Lopez L, Rodriguez-Cuevas J, Martinez-Lopez J, Martyniuk A. A multilayer circular polarizer based on bisected split-ring frequency selective surfaces. *IEEE Antennas Wireless Propag Lett* 2014;13:153–6.
- [29] Gao J, Zhang K, Yang G, Wu Q. A novel four-face polarization twister based on three-dimensional magnetic toroidal dipoles. *IEEE Trans Magn* 2014;50:1–4.
- [30] Wu L, Yang Z, Cheng Y, et al. Circular polarization converters based on bi-layered asymmetrical split ring metamaterials. *Appl Phys A* 2014;116:643–8.
- [31] Jiang S-C, Xiong X, Hu Y-S, et al. Controlling the polarization state of light with a dispersion-free metastructure. *Phys Rev X* 2014;4:021026.
- [32] Huang C, Ma X, Pu M, Yi G, Wang Y, Luo X. Dual-band 90° polarization rotator using twisted split ring resonators array. *Opt Commun* 2013;291:345–8.
- [33] Zhao J-X, Xiao B-X, Huang J-X, Yang H-L. Multiple-band reflective polarization converter based on complementary L-shaped metamaterial. *Microw Opt Technol Lett* 2015;57:978–83.
- [34] Levesque Q, Makhsiyani M, Bouchon P, et al. Plasmonic planar antenna for wideband and efficient linear polarization conversion. *Appl Phys Lett* 2014;104:111105.
- [35] Kenanakis G, Zhao R, Stavrinidis A, et al. Flexible chiral metamaterials in the terahertz regime: a comparative study of various designs. *Opt Mater Express* 2012;2:1702–12.
- [36] Li M, Guo L, Dong J, Yang H. An ultra-thin chiral metamaterial absorber with high selectivity for LCP and RCP waves. *J Phys D* 2014;47:185102.
- [37] Bian B, Liu S, Wang S, et al. Novel triple-band polarization-insensitive wide-angle ultra-thin microwave metamaterial absorber. *J Appl Phys* 2013;114:194511.
- [38] Valagiannopoulos CA, Tukiainen A, Aho T, et al. Perfect magnetic mirror and simple perfect absorber in the visible spectrum. *Phys Rev B* 2015;91:115305.
- [39] Wen Y, Ma W, Bailey J, Matmon G, Yu X, Aeppli G. Planar broadband and high absorption metamaterial using single nested resonator at terahertz frequencies. *Opt Lett* 2014;39:1589–92.
- [40] Dincer F, Akgol O, Karaaslan M, Unal E, Sabah C. Polarization angle independent perfect metamaterial absorbers for solar cell applications in the microwave, infrared, and visible regime. *Prog Electromagn Res* 2014;144:93–101.
- [41] Yoo M, Lim S. Polarization-independent and ultrawideband metamaterial absorber using a hexagonal artificial impedance surface and a resistor-capacitor layer. *IEEE Trans Antennas Propag* 2014;62:2652–8.
- [42] Ra'di Y, Asadchy V, Tretyakov S. Total absorption of electromagnetic waves in ultimately thin layers. *IEEE Trans Antennas Propag* 2013;61:4606–14.
- [43] Yu N, Genevet P, Kats MA, et al. Light propagation with phase discontinuities: generalized laws of reflection and refraction. *Science* 2011;334:333–7.
- [44] Yu N, Capasso F. Flat optics with designer metasurfaces. *Nat Mater* 2014;13:139–50.
- [45] Genevet P, Capasso F. Breakthroughs in photonics 2013: flat optics: wavefronts control with Huygens' interfaces. *Photon J IEEE* 2014;6:1–4.
- [46] Shi J, Fang X, Rogers ETF, Plum E, MacDonald KF, Zheludev NI. Coherent control of Snell's law at metasurfaces. *Opt Express* 2014;22:21051–60.
- [47] Yang Q, Gu J, Wang D, et al. Efficient flat metasurface lens for terahertz imaging. *Opt Express* 2014;22:25931–9.
- [48] Asadchy S, Ra'di YV, Vehmas J, Tretyakov A. Functional metamirrors using bianisotropic elements. *Phys Rev Lett* 2015;114:095503.
- [49] Lipworth G, Mrozack A, Hunt J, et al. Metamaterial apertures for coherent computational imaging on the physical layer. *J Opt Soc Am A* 2013;30:1603–12.
- [50] Hunt J, Driscoll T, Mrozack A, et al. Metamaterial apertures for computational imaging. *Science* 2013;339:310–3.
- [51] Liu F, Xiao S, Sihvola A, Li J. Perfect co-circular polarization reflector: a class of reciprocal perfect conductors with total co-circular polarization reflection. *IEEE Trans Antennas Propag* 2014;62:6274–81.
- [52] Germain D, Seetharamdoo D, Nawaz Burokur S, de Lustrac A. Phase-compensated metasurface for a conformal microwave antenna. *Appl Phys Lett* 2013;103:124102.
- [53] Holloway CL, Love DC, Kuester EF, Salandrino A, Engheta N. Sub-wavelength resonators: on the use of metafilms to overcome the  $\lambda$  size limit. *IET Microw Antennas Propag* 2008;2:120–9.
- [54] Ra'di Y, Asadchy V, Tretyakov S. Tailoring reflections from thin composite metamirrors. *IEEE Trans Antennas Propag* 2014;62:3749–60.
- [55] Abdelrahman A, Elsherbeni A, Yang F. Transmitarray antenna design using cross-slot elements with no dielectric substrate. *IEEE Antennas Wireless Propag Lett* 2014;13:177–80.
- [56] Shi H, Li J, Zhang A, et al. Gradient metasurface with both polarization-controlled directional surface wave coupling and anomalous reflection. *IEEE Antennas Wireless Propag Lett* 2015;14:104–7.
- [57] Nye J, Berry M. Dislocations in wave trains. *Proc R Soc A Math Phys Eng Sci* 1974;336:165–90.
- [58] Karimi E, Schulz SA, De Leon I, Qassim H, Upham J, Boyd RW. Generating optical orbital angular momentum at visible wavelengths using a plasmonic metasurface. *Light Sci Appl* 2014;3:e167.
- [59] Pfeiffer C, Grbic A. Controlling vector Bessel beams with metasurfaces. *Phys Rev Appl* 2014;2:044012.
- [60] Yi X, Ling X, Zhang Z, et al. Generation of cylindrical vector vortex beams by two cascaded metasurfaces. *Opt Express* 2014;22:17207–15.
- [61] Veysi M, Guclu C, Capolino F. Vortex beams with strong longitudinally polarized magnetic field and their generation by using metasurfaces. *J Opt Soc Am B* 2015;32:345–54.
- [62] Sun J, Wang X, Xu T, Kudyshev ZA, Cartwright AN, Litchinitser NM. Spinning light on the nanoscale. *Nano Lett* 2014;14:2726–9.
- [63] Lin J, Genevet P, Kats MA, Antoniou N, Capasso F. Nanostructured holograms for broadband manipulation of vector beams. *Nano Lett* 2013;13:4269–74.

- [64] Hunt J, Gollub J, Driscoll T, et al. Metamaterial microwave holographic imaging system. *J Opt Soc Am A* 2014;31:2109–19.
- [65] Zheng G, Mühlenbernd H, Kenney M, Li G, Zentgraf T, Zhang S. Metasurface holograms reaching 80% efficiency. *Nat Nanotechnol* 2015;10:308–12.
- [66] Pfeiffer C, Grbic A. Generating stable tractor beams with dielectric metasurfaces. *Phys Rev B* 2015;91:115408.
- [67] Da H, Bao Q, Sanaei R, et al. Monolayer graphene photonic metastructures: giant Faraday rotation and nearly perfect transmission. *Phys Rev B* 2013;88:205405.
- [68] Degiron A, Smith DR. One-way glass for microwaves using nonreciprocal metamaterials. *Phys Rev E* 2014;89:053203.
- [69] Ra'di Y, Asadchy VS, Tretyakov SA. One-way transparent sheets. *Phys Rev B* 2014;89:075109.
- [70] Kodera T, Sounas DL, Caloz C. Artificial Faraday rotation using a ring metamaterial structure without static magnetic field. *Appl Phys Lett* 2011;99:031114.
- [71] Sounas D, Kodera T, Caloz C. Electromagnetic modeling of a magnetless nonreciprocal gyrotropic metasurface. *IEEE Trans Antennas Propag* 2013;61:221–31.
- [72] Zhu Y, Hu X, Chai Z, Yang H, Gong Q. Active control of chirality in nonlinear metamaterials. *Appl Phys Lett* 2015;106:091109.
- [73] Valev VK, Baumberg J, De Clercq B, et al. Nonlinear superchiral meta-surfaces: tuning chirality and disentangling non-reciprocity at the nanoscale. *Adv Mater* 2014;26:4074–81.
- [74] Lee J, Tymchenko M, Argyropoulos C, et al. Giant nonlinear response from plasmonic metasurfaces coupled to intersubband transitions. *Nature* 2014;511:65–9.
- [75] Pors A, Nielsen MG, Bozhevolnyi SI. Analog computing using reflective plasmonic metasurfaces. *Nano Lett* 2015;15:791–7.
- [76] Silva A, Monticone F, Castaldi G, Galdi V, Alù A, Engheta N. Performing mathematical operations with metamaterials. *Science* 2014;343:160–3.
- [77] Ortiz J, Baena J, Losada V, Medina F, Araque J. Spatial angular filtering by FSSs made of chains of interconnected SRRs and CSRRs. *IEEE Microw Compon Lett* 2013;23:477–9.
- [78] Shen Y, Ye D, Wang L, et al. Metamaterial broadband angular selectivity. *Phys Rev B* 2014;90:125422.
- [79] Shen Y, Ye D, Celanovic I, Johnson SG, Joannopoulos JD, Soljačić M. Optical broadband angular selectivity. *Science* 2014;343:1499–501.
- [80] Achouri K, Salem MA, Caloz C. General metasurface synthesis based on susceptibility tensors. *IEEE Trans Antennas Propag* 2015;63:2977–91.
- [81] Salem MA, Achouri K, Caloz C. Metasurface synthesis for time-harmonic waves: exact spectral and spatial methods. *Prog Electromagn Res* 2014;149:205–16.
- [82] Salem MA, Caloz C. Manipulating light at distance by a metasurface using momentum transformation. *Opt Express* 2014;22:14530–43.
- [83] Pfeiffer C, Emani NK, Shaltout AM, Boltasseva A, Shalaev VM, Grbic A. Efficient light bending with isotropic metamaterial Huygens' surfaces. *Nano Lett* 2014;14:2491–7.
- [84] Pfeiffer C, Grbic A. Metamaterial Huygens' surfaces: tailoring wave fronts with reflectionless sheets. *Phys Rev Lett* 2013;110:197401.
- [85] Pfeiffer C, Grbic A. Millimeter-wave transmitarrays for wave-front and polarization control. *IEEE Trans Microw Theory Tech* 2013;61:4407–17.
- [86] Pfeiffer C, Grbic A. Bianisotropic metasurfaces for optimal polarization control: analysis and synthesis. *Phys Rev Appl* 2014;2:044011.
- [87] Wong JP, Selvanayagam M, Eleftheriades GV. Design of unit cells and demonstration of methods for synthesizing Huygens metasurfaces. *Photon Nanostruct Fundam Appl* 2014;12:360–75, *Metamaterials-2013 Congress*.
- [88] Selvanayagam M, Eleftheriades G. Polarization control using tensor Huygens surfaces. *IEEE Trans Antennas Propag* 2014;62:6155–68.
- [89] Epstein A, Eleftheriades G. Passive lossless Huygens metasurfaces for conversion of arbitrary source field to directive radiation. *IEEE Trans Antennas Propag* 2014;62:5680–95.
- [90] Niemi T, Karilainen A, Tretyakov S. Synthesis of polarization transformers. *IEEE Trans Antennas Propag* 2013;61:3102–11.
- [91] Idemen MM. *Discontinuities in the electromagnetic field*. Chichester, UK, John Wiley & Sons, 2011.
- [92] Albooyeh M, Tretyakov S, Simovski C. Electromagnetic characterization of bianisotropic metasurfaces on refractive substrates: general theoretical framework. *Ann Phys* 2016;528:721–37.
- [93] Kong J. *Electromagnetic wave theory*. Ser. A Wiley-Interscience publication. Chichester, UK, John Wiley & Sons, 1986.
- [94] Sihvola AH, Viitanen AJ, Lindell IV, Tretyakov SA. *Electromagnetic waves in chiral and bi-isotropic media*. Ser. The Artech House Antenna Library. Artech House, 1994.
- [95] Serdiukov A, Semchenko I, Tertyakov S, Sihvola A. *Electromagnetics of Bi-anisotropic Materials – Theory and Application*. Amsterdam, Gordon and Breach Science Publishers, 2001. vol. 11.
- [96] Achouri K, Vahabzadeh Y, Caloz C. Mathematical synthesis and analysis of a second-order magneto-electrically nonlinear metasurface. *Opt Express* 2017;25:19013–22.
- [97] Kuester EF, Mohamed M, Piket-May M, Holloway C. Averaged transition conditions for electromagnetic fields at a metafilm. *IEEE Trans Antennas Propag* 2003;51:2641–51.
- [98] Achouri K, Khan BA, Gupta S, Lavigne G, Salem MA, Caloz C. Synthesis of electromagnetic metasurfaces: principles and illustrations. *EPJ Appl Metamater* 2015;2:12.
- [99] Achouri K, Salem MA, Caloz C. Electromagnetic metasurface performing up to four independent wave transformations. In: *2015 IEEE Conference on Antenna Measurements Applications (CAMA) 2015:1–3*.
- [100] Vahabzadeh Y, Chamanara N, Achouri K, Caloz C. Computational analysis of metasurfaces. *arXiv preprint arXiv:1710.11264*, 2017.
- [101] Saleh B, Teich M. *Fundamentals of photonics, wiley series in pure and applied optics*. New York, Wiley, 2007.
- [102] Sounas DL, Caloz C. Electromagnetic non-reciprocity and gyrotropy of graphene. *Appl Phys Lett* 2011;98:1–3.
- [103] Albooyeh M, Kazemi H, Capolino F, Kwon DH, Tretyakov SA. Normal vs tangential polarizations in metasurfaces. In: *2017 IEEE International Symposium on Antennas and Propagation, USNC/URSI National Radio Science Meeting 2017:1707–8*.
- [104] Gordon JA, Holloway CL, Dienstfrey A. A physical explanation of angle-independent reflection and transmission properties of metafilms/metamaterials. *IEEE Antennas Wireless Propag Lett* 2009;8:1127–30.
- [105] Di Falco A, Zhao Y, Alù A. Optical metasurfaces with robust angular response on flexible substrates. *Appl Phys Lett* 2011;99:163110.

- [106] Ra'di Y, Tretyakov S. Angularly-independent Huygens' metasurfaces. In: 2015 IEEE International Symposium on Antennas and Propagation & USNC/URSI National Radio Science Meeting. IEEE 2015:874–75.
- [107] Kildishev AV, Borneman JD, Ni X, Shalaev VM, Drachev VP. Bianisotropic effective parameters of optical metamagnetics and negative-index materials. *Proc IEEE* 2011;99:1691–700.
- [108] Nakata Y, Urade Y, Nakanishi T, Kitano M. Plane-wave scattering by self-complementary metasurfaces in terms of electromagnetic duality and Babinet's principle. *Phys Rev B* 2013;88:205138.
- [109] Asadchy VS, Fanyayev IA. Simulation of the electromagnetic properties of helices with optimal shape, which provides radiation of a circularly polarized wave. *J Adv Res Phys* 2011;2.
- [110] Asadchy VS, Faniayev IA, Ra'di Y, Tretyakov SA. Determining polarizability tensors for an arbitrary small electromagnetic scatterer. *Photon Nanostruct Fundam Appl* 2014;12:298–304.
- [111] Berreman DW. Optics in stratified and anisotropic media: 44-matrix formulation. *J Opt Soc Am* 1972;62:502–10.
- [112] Dmitriev V. Group theoretical approach to complex and bianisotropic media description. *Eur Phys J AP* 1999;6:49–55.
- [113] Reinke CM, De la Mata Luque TM, Su MF, Sinclair MB, El-Kady I. Group-theory approach to tailored electromagnetic properties of metamaterials: an inverse-problem solution. *Phys Rev E* 2011;83:066603.
- [114] Kruk SS, Poddubny AN, Powell DA, et al. Polarization properties of optical metasurfaces of different symmetries. *Phys Rev B* 2015;91:195401.
- [115] Pfeiffer C, Zhang C, Ray V, Guo LJ, Grbic A. High performance bianisotropic metasurfaces: asymmetric transmission of light. *Phys Rev Lett* 2014;113:023902.
- [116] Epstein A, Eleftheriades GV. Arbitrary power-conserving field transformations with passive lossless omega-type bianisotropic metasurfaces. *IEEE Trans Antennas Propag* 2016;64:3880–95.
- [117] Wong JPS, Epstein A, Eleftheriades GV. Reflectionless wide-angle refracting metasurfaces. *IEEE Antennas Wireless Propag Lett* 2016;15:1293–6.
- [118] Lin D, Fan P, Hasman E, Brongersma ML. Dielectric gradient metasurface optical elements. *Science* 2014;345:298–302.
- [119] Arbabi A, Horie Y, Bagheri M, Faraon A. Dielectric metasurfaces for complete control of phase and polarization with subwavelength spatial resolution and high transmission. *Nat Nanotechnol* 2015;10:937–43.
- [120] Krasnok A, Makarov S, Petrov M, Savelev R, Belov P, Kivshar Y. Towards all-dielectric metamaterials and nanophotonics. *Proc SPIE* 2015;9502:950203–17.
- [121] Aieta F, Kats MA, Genevet P, Capasso F. Multiwavelength achromatic metasurfaces by dispersive phase compensation. *Science* 2015;347:1342–5.
- [122] Achouri K, Lavigne G, Caloz C. Comparison of two synthesis methods for birefringent metasurfaces. *J Appl Phys* 2016;120:235305.
- [123] Lavigne G, Achouri K, Asadchy V, Tretyakov S, Caloz C. Refracting metasurfaces without spurious diffraction. *arXiv preprint arXiv:1705.09286v2*, 2017.
- [124] Chen L, Achouri K, Kallos E, Caloz C. Simultaneous enhancement of light extraction and spontaneous emission using a partially reflecting metasurface cavity. *Phys Rev A* 2017;95:053808.
- [125] Achouri K, Lavigne G, Salem MA, Caloz C. Metasurface spatial processor for electromagnetic remote control. *IEEE Trans Antennas Propag* 2016;64:1759–67.
- [126] Taravati S, Khan BA, Gupta S, Achouri K, Caloz C. Nonreciprocal nongyrotropic magnetless metasurface. *IEEE Trans Antennas Propag* 2017;65:1.
- [127] Achouri K, Yahyaoui A, Gupta S, Rmili H, Caloz C. Dielectric resonator metasurface for dispersion engineering. *IEEE Trans Antennas Propag* 2017;65:673–80.
- [128] Achouri K, Caloz C. Metasurface solar sail for flexible radiation pressure control, *arXiv preprint arXiv:1710.02837*, 2017.